Aerosol Science and Technology
Publication details, including instructions for authors and subscription information:
http://www.tandfonline.com/loi/uast20

Similarities in STXM-NEXAFS Spectra of Atmospheric Particles and Secondary Organic Aerosol Generated from Glyoxal, α-Pinene, Isoprene, 1,2,4-Trimethylbenzene, and d-Limonene

Kabindra M. Shakya [a b], Shang Liu [a], Satoshi Takahama [a c], Lynn M. Russell [a], Frank N. Keutsch [d], Melissa M. Galloway [d e], John E. Shilling [f], Naruki Hiranuma [f g], Chen Song [f], Hwajin Kim [h], Suzanne E. Paulson [h], Lisa Pfaffenberger [i], Peter Barmet [i], Jay Slowik [i], André S. H. Prévôt [i], Josef Dommen [i] & Urs Baltensperger [i]

[a] Scripps Institution of Oceanography, University of California, San Diego, La Jolla, California, USA

[b] Now at Division of Environmental Health, Department of Public Health, School of Public Health Sciences, University of Massachusetts, Amherst, Massachusetts, USA

[c] Now at Ecole Polytechnique Federale De Lausanne, Switzerland

[d] Department of Chemistry, University of Wisconsin-Madison, Madison, Wisconsin, USA

[e] Now at Department of Chemistry and Biochemistry, University of San Diego, California, X, USA

[f] Atmospheric Sciences and Global Change Division, Pacific Northwest National Laboratory, Richland, Washington, USA

[g] Now at Institute for Meteorology and Climate Research, Karlsruhe Institute of Technology, Germany

[h] Division of Atmospheric and Oceanic Sciences, University of California at Los Angeles, California, X, USA

[i] Laboratory of Atmospheric Chemistry, Paul Scherrer Institute, Switzerland

Accepted author version posted online: 06 Feb 2013.

Similarities in STXM-NEXAFS Spectra of Atmospheric Particles and Secondary Organic Aerosol Generated from Glyoxal, α-Pinene, Isoprene, 1,2,4-Trimethylbenzene, and d-Limonene

Kabindra M. Shakya[1,2], Shang Liu[1], Satoshi Takahama[1,3], Lynn M. Russell[1], Frank N. Keutsch[4], Melissa M. Galloway[4,5], John E. Shilling[6], Naruki Hiranuma[6,7], Chen Song[6], Hwajin Kim[8], Suzanne E. Paulson[8], Lisa Pfaffenberger[9], Peter Barmet[9], Jay Slowik[9], André S. H. Prévôt[9], Josef Dommen[9], Urs Baltensperger[9]

[1]Scripps Institution of Oceanography, University of California, San Diego, La Jolla, California, USA

[2]Now at Division of Environmental Health, Department of Public Health, School of Public Health Sciences, University of Massachusetts, Amherst, Massachusetts, USA

[3]Now at Ecole Polytechnique Federale De Lausanne, Switzerland

[4]Department of Chemistry, University of Wisconsin-Madison, Madison, Wisconsin, USA

[5]Now at Department of Chemistry and Biochemistry, University of San Diego, California, USA

[6]Atmospheric Sciences and Global Change Division, Pacific Northwest National Laboratory, Richland, Washington, USA

[7]Now at Institute for Meteorology and Climate Research, Karlsruhe Institute of Technology, Germany

[8]Division of Atmospheric and Oceanic Sciences, University of California at Los Angeles, California, USA

[9]Laboratory of Atmospheric Chemistry, Paul Scherrer Institute, Switzerland

Address correspondence to Lynn M. Russell, Scripps Institute of Oceanography, University Of California-San Diego, 9500 Gilman Drive, La Jolla, CA 92093-0221. E-mail: lmrussell@ucsd.edu

ABSTRACT

The organic functional group composition of particles produced in laboratory "smog" chambers were characterized by scanning transmission X-ray microscopy (STXM) with near-edge X-ray absorption fine structure (NEXAFS) spectroscopy and characteristic spectral signatures for secondary organic aerosol (SOA) were identified. The main objective of this study is to compare the single particle functional group composition of SOA formed from five precursors (glyoxal, α-pinene, isoprene, 1,2,4-trimethylbenzene, and d-limonene) to the composition of ambient particles from multiple field campaigns. This has implications in understanding the potential contributions of particles similar to those produced in SOA chambers to ambient compositions during those campaigns. Glyoxal uptake studies showed absorption from mainly alkyl, carbon-nitrogen (C-N), and carboxylic carbonyl groups. The SOA formed from the photooxidation of α-pinene (with and without isoprene) showed stronger absorptions for alkyl and carbonyl groups than the SOA formed from glyoxal. The mass ratio of carbonyl to acid group was larger in α-pinene-only experiments relative to the mixed α-pinene-isoprene experiments. Of 338 single-particle spectra available from aerosol sampling at six field campaigns, 114 particles had spectral features that were considered similar to the chamber-SOA particles: MILAGRO-2006 (9 particles), VOCALS-2008 (41 particles), Whistler-2008 (22 particles), Scripps Pier-2009 (8 particles), Bakersfield-2010 (24 particles), and Whistler-2010

(10 particles). These similarities with chamber-generated SOA provide spectroscopic evidence of chemically similar SOA products from these precursors in ambient particles.

1. INTRODUCTION

Secondary organic aerosol (SOA) particles are formed by a combination of homogeneous nucleation and condensation of low volatility oxidation products. SOA consists of compounds containing multiple functional groups (e.g. hydroxyl, ketonic, aldehydic, and carboxylic carbonyl), which affect their polarity and volatility (Kroll and Seinfeld 2008). SOA formation has been studied extensively in laboratory chambers; it is now well established that SOA formation generally involves multiple generations of oxidation that include both functionalization and fragmentation steps (Ng et al. 2006; Madrid et al. 2010; Yee et al. 2012).

Monoterpenes (e.g. α-pinene, limonene), other terpenoid compounds (e.g. isoprene), and aromatic hydrocarbons (such as toluene and 1,2,4-trimethylbenzene (TMB)) are volatile organic compounds (VOCs) that are precursors to biogenic and anthropogenic SOA formation (Griffin et al. 1999; Kanakidou et al. 2005; Henze and Seinfeld 2006). Isoprene and monoterpenes account for about 50% and 11% of the natural biogenic VOC emissions, respectively; α-pinene and limonene contribute ~25% and ~16%, respectively, of monoterpene emissions (Kanakidou et al. 2005). Limonene, α-pinene, and TMB have higher SOA yields than isoprene, however, isoprene is the more important SOA source globally due to its higher emissions (Griffin et al. 1999; Kanakidou et al. 2005; Paulsen et al. 2005). It has been suggested that glyoxal (a dicarbonyl generated from the atmospheric oxidation of aromatics, acetylene, and biogenic hydrocarbons (Jang and Kamens 2001; Fu et al. 2008)) contributes to ambient organic aerosol concentrations

(Volkamer et al. 2007; Washenfelder et al. 2011). However, its contribution depends on meteorological conditions, and it was not observed to be significant to aerosol formation in the dry conditions of the BEARPEX 2007 campaign in the Sierra Nevada Mountains (Huisman et al. 2011). In the aqueous phase, glyoxal is largely hydrated and it can react with another glyoxal molecule, ammonium, or alcohol to generate new products that include oligomers, acetals, imidazoles, and organic acids (Liggio et al. 2005; De Haan et al., 2009; Galloway et al. 2009; Ervens et al. 2011; Yu et al. 2011). Chamber studies on SOA from various precursors have shown SOA formed from glyoxal uptake contains higher O:C ratios (elemental oxygen to carbon ratio) compared to other SOA precursors such as α-pinene, isoprene, and aromatics (Chhabra et al. 2010).

Organic aerosols comprise a mixture of a large number of compounds, many of which have not been identified. Functional group analysis by scanning transmission X-ray microscopy with near edge X-ray absorption fine structure (STXM-NEXAFS) spectroscopy can identify organic functional groups in both chamber-generated and ambient aerosol in single particles. Using another functional-group-based approach, Russell et al. (2011) showed that the Fourier transform infrared (FTIR) spectra of atmospheric particles exhibit compositions similar to those of chamber-generated particles. In particular, the FTIR spectra of aerosols from many urban-influenced regions show similar amounts of alkane, carboxylic acid, and alcohol functional groups to chamber SOA from alkane photooxidation, and particles from biogenically-influenced field campaigns were similar to chamber SOA from α-pinene photooxidation.

STXM-NEXAFS is an important technique for analyzing the chemical composition, size, and morphology of atmospheric particles (Russell et al. 2002; Takahama et al. 2007, 2010). This

method has an advantage over other electron microscopy techniques (e.g. electron energy loss spectroscopy) of causing less damage to the sample and not requiring sectioning. Takahama et al. (2007) applied a cluster analysis algorithm to STXM data to classify ambient particles collected from multiple field campaigns into 14 particle types, including combustion-, SOA-, dust-, and soot-type particles. This classification has been used to distinguish STXM-derived particle types in several field campaigns (Day et al. 2009; Liu et al. 2009, 2011; Schwartz et al. 2010; Hawkins et al. 2010). Recently, Takahama et al. (2011) also observed biomass burning type particles (amorphous carbon tarballs) with strong absorption from a ketone group.

In this study we use STXM-NEXAFS spectroscopy of single particles to compare the functional group composition of SOA particles formed from five precursors to the composition of ambient single particles. This comparison allows us to identify which, if any, of the precursors used in chamber experiments are consistent with SOA particles measured in the atmosphere. First, we summarize the morphology and composition of SOA formed from photooxidation of biogenic (α-pinene, isoprene, and d-limonene) and anthropogenic (1,2,4-trimethylbenzene) SOA precursors and from aerosol uptake of glyoxal. Then we use these chamber-generated particle spectra as reference standards, against which we compare the spectra of atmospheric particles from six prior field campaigns: Megacity Initiative: Local and Global Research Observations (MILAGRO), VAMOS Ocean-Cloud-Atmosphere-Land Study (VOCALS), Scripps Pier, Bakersfield (CalNex), and Whistler, British Columbia (during 2008 and 2010).

2. METHODS

2.1 Laboratory chamber SOA

Four laboratory chambers of different volumes were utilized to produce the SOA investigated here in a controlled environment: glyoxal at the California Institute of Technology (Caltech, 28 m^3), α-pinene and isoprene at the Paul Scherrer Institute (PSI, 27 m^3), 1,2,4-trimethylbenzene at Pacific Northwest National Laboratory (PNNL, 10.6 m^3), and d-limonene at University of California, Los Angeles (UCLA, 24 m^3). The glyoxal chamber experiments used four types of seed aerosol, the α-pinene and isoprene experiments used one type of seed aerosol, and the 1,2,4-trimethylbenzene and d-limonene experiments used no seed aerosol. Table 1 provides additional information about the SOA precursors, seeds, relative humidity, and light conditions.

The experimental design of the glyoxal uptake experiments in the Caltech chamber was analogous to that described by Galloway et al. (2009). Four types of seed particles were used: ammonium bisulfate (NH_4HSO_4), magnesium sulfate and sulfuric acid ($MgSO_4$+H_2SO_4), sodium nitrate ($NaNO_3$), and sodium sulfate (Na_2SO_4). Glyoxal was injected into the chamber before introducing the seeds, which were generated by atomization of aqueous inorganic solution of the respective seed types. Glyoxal was introduced by vaporization of the glyoxal monomer generated from a mixture of glyoxal trimer dihydrate (Sigma Aldrich, >97%) and phosphorus pentoxide. Glyoxal concentrations ranging from 27 to 38.5 ppbv were used in the experiments. Lights were not turned on so that uptake was measured without photochemical reactions, and relative humidity was maintained at around 70% (Table 1).

Two photooxidation experiments, one with mixing ratios of 45 ppbv α-pinene and one with 40 ppbv α-pinene together with 400 ppbv isoprene were performed in the PSI chamber.

The chamber design is described in Paulsen et al. (2005), and further details of the experiments are presented in Pfaffenberger et al. (2012). Black carbon (BC, Tokai Black) and ammonium bisulfate were injected as seed aerosol to investigate SOA composition as a function of hygroscopicity. HONO was injected continuously throughout the experiment and via photolysis served as a source of both nitrogen oxides (NO_x) and hydroxyl radical (OH) once the UV and xenon lights were switched on. On February 11, 2011, 50 ppbv of NO were additionally injected at the beginning and at a continuous rate (1005 ppmv ± 2%, purity: 99.8%, flow rate: 10-105 ml min^{-1}) during the whole experiment time. The NO addition led to a concentration of 4-45 ppbv NO_2 and 1-50 ppbv NO (Table 1).

Photooxidation experiments for 1,2,4-trimethylbenzene (Sigma-Aldrich) were performed in the PNNL chamber. The oxidant (OH) was generated from the photolysis of HONO that was prepared from the reaction of $NaNO_2$ (Sigma-Aldrich; ≥ 97%) and H_2SO_4 (Sigma-Aldrich; 99.999%). No seed aerosols were used. Particles were collected from the experiment performed with 300 ppbv of 1,2,4-TMB and 2000 ppbv of HONO, maintained at the relative humidity of 15 to 20% (Table 1). Details of the PNNL experiments are given in Liu et al. (2012a).

The d-limonene photooxidation experiment was performed in a chamber exposed to natural sunlight at the University of California, Los Angeles (UCLA). d-Limonene (Aldrich, 99.8%) at 190 ppbv was injected into the chamber. It was a "high NO_x" experiment with 290 ppbv of NO_x and HC/NO_x ratio (ppbC/ppb) of 6.6. No seed aerosols were used. Relative humidity was maintained at 24-39%. Experimental conditions are also given in Table 1.

2.2 Sampling

In each case, particles were collected on silicon nitride windows (Si_3N_4, Silson Ltd.) by utilizing the top stage of a rotating impactor (Streaker, PIXE International, Inc.). Sampling duration ranged from 10 min to 1 hr at a flow rate of 1 L min^{-1}. Tubing made of either aluminum or copper was used to draw air into the impactor. All samples were frozen after collection, and stored cold (<0 ^{o}C) until analysis.

2.3 STXM-NEXAFS

Particles were analyzed at the Advanced Light Source (ALS) of Lawrence Berkeley National Laboratory (Berkeley, CA). Beamline 5.3.2 with a He-filled chamber maintained at 1 atm was used for analysis. Particles were scanned for energy levels between 278 and 320 eV (0.2–5 eV step size) to obtain X-ray absorption spectra of the carbon K-edge. Organic carbon-containing functional groups were identified based on their specific absorption energy range: aromatic or alkene (284.4-286.4 eV: C 1s - $\pi^*_{C=C}$), ketone (286.5-286.9 eV: C 1s - $\pi^*_{C=O}$), alkyl (287.4-288.5 eV: C 1s - σ^*_{C-H}; 290.8-293 eV: C 1s - σ^*_{C-C}), amide carbonyl (288.3±0.2 eV: C 1s - $\pi^*_{C=O}$), carboxylic carbonyl (288.2-288.9 eV: C 1s - $\pi^*_{C=O}$), and alcohol (289.5±0.3 eV: C 1s - $3p/\sigma^*_{C-OH}$) (Russell et al. 2002; Takahama et al. 2007, 2010; Cody et al., 2008; Hawkins and Russell 2010). Details on peak fitting and STXM-NEXAFS data processing are given elsewhere (Russell et al. 2002; Takahama et al. 2007, 2010). Spectra collected at the ALS were analyzed using MATLAB codes described by Takahama et al. (2010) after pre-processing by aXis2000 software (Hitchcock 2000). The pre-edge background (mean value between 278 and 283 eV) was subtracted from all spectra, which were then normalized by the carbon K-edge absorbance (mean value between 305 and 320 eV) to compare the spectral differences based on

chemical structure (Tivanski et al. 2007; Takahama et al. 2010). The distribution of different chemical components, within and among particles, and the particle aspect ratios were estimated using algorithms reported by Takahama et al. (2010).

2.4 Comparison of particle spectra

Laboratory chamber particle spectra were compared with ambient particle spectra collected from multiple field campaigns. The comparisons were also made for the spectra types classified by Takahama et al. (2007). The field campaigns include MILAGRO, VOCALS, Bakersfield (CalNex), Scripps Pier, and Whistler. Details on the study locations and periods are given in Table 2. Evaluation of the similarity of spectra is based on the cosine angle metric and examination of the similarity of main peaks. The cosine angle metric (Cosθ) measures the dot product of two spectral vectors (Tabb et al. 2003):

$$\cos\theta = \frac{\sum i_1 i_2}{\sqrt{\sum i_1^2 \sum i_2^2}} \quad (1)$$

where i_1 and i_2 denote spectral vectors of two single particles (e.g. particle 1 from a chamber experiment and particle 2 from an ambient measurement). The cosine angle metric was calculated for absorbance in the energy range of 286-294 eV; wider energy ranges include more influence from seed particles and noise. Spectra were matched based on both the calculated cosine angle metrics (greater than 0.9) and a visual comparison of overlaid spectra (at least two common peaks). Only those spectra with cosine angle metric greater than 0.9 are considered "similar" in the comparisons that follow.

3. RESULTS AND DISCUSSION

Here we present the STXM-NEXAFS spectral characteristics of 75 particles formed from five different precursors in chamber experiments and discuss the implications of the spectra for the chemical composition of the SOA formed. Then, we compare the spectra of these chamber-generated particles to those of 338 ambient particles from six field campaigns. We identified 114 ambient particles (summarized in Table 2), 43 of which had been classified previously as "secondary" (type "a" in Takahama et al., 2007), that were "similar" (cosine angle metric greater than 0.9 and two common peaks) to one of the five types of chamber SOA studied here. There were 224 other particles analyzed by STXM-NEXAFS during these 6 campaigns, 59 of which had been previously classified as this same "secondary" type that did not have sufficiently similar spectral features to the SOA particles formed in chamber experiments.

3.1 Laboratory chamber SOA

Figure 1 shows the average STXM-NEXAFS spectra of SOA particles formed during the different chamber experiments.

3.1.1 Glyoxal uptake

Spectral profiles of particles generated from glyoxal uptake differed as a function of seed type (Figure 1a, 1b, and 1d), although most particles from these glyoxal chamber studies had distinct spectral peaks corresponding to alcohol, amide carbonyl, and alkyl groups. The most distinguishing feature is the presence of groups containing carbon and nitrogen, which is particularly clear in the experiment with NH_4HSO_4 seed (Figure 1a). However, the carboxylic

carbonyl group overlaps with the amide group absorption region, so the identification of the amide group is not certain. The spectra of particles generated from glyoxal uptake on Na_2SO_4 seeds are characterized by two distinct peaks for carboxylic carbonyl and alkyl groups.

The alkyl group peak at ~291 eV was more pronounced in the experiments with $MgSO_4$+H_2SO_4, $NaNO_3$, and Na_2SO_4 seeds (Figure 1). The peak at (290.6-291 eV) has been assigned to lower energy σ* (C-C) transitions associated with the larger number of carbon-carbon single bonds in a study of organocobalt complexes by inner-shell electron energy loss spectrometry (Rühl et al. 1991). Geminal diols, acetals, and hydrated glyoxal units are one of the major reaction products in the glyoxal uptake experiments (Liggio et al. 2005). However, the expected signals at ~289.5 eV for hydroxyl functional groups were not observed except in the experiments with NH_4HSO_4 and $MgSO_4$+H_2SO_4 seeds. The peaks at ~290.9 eV in all the glyoxal experiments might also be assigned to the hydroxyl functional groups as the signals from alcohols are also observed at ~291 eV (Myneni 2002). The proposed structures of glyoxal fragments (e.g. mass to charge ratio: 44, 58, 135, 145, and 175) obtained by aerosol mass spectrometry from a similar series of glyoxal uptake experiments onto ammonium sulfate seed aerosol were given by Galloway et al. (2009). Products such as imidazoles, carboxaldehyde, formic acid and acetic acids have been observed from the reaction of glyoxal and ammonium in aqueous solution (Yu et al. 2011). The final SOA products will differ based on the pathways of heterogeneous reactions of glyoxal (Liggio et al. 2005).

The spectra in the presence of NH_4HSO_4 seeds are different from others due to absorption in the region of carbon-nitrogen containing groups. In addition to the amide carbonyl group, the spectra from these particles also exhibit shoulders in the region of 287.0-287.9 eV. Absorptions

in the region of 287.0-287.9 eV are also reported for compounds containing the imidazole group (Solomon et al. 2009, 2012). Several carbon-nitrogen (C-N) containing compounds, including imidazole, imidazole-2-carboxaldehyde, and 1N-glyoxal-substituted imidazole, and formic and acetic acids have been identified from the reaction of glyoxal and ammonium (Nozière et al. 2009; Yu et al. 2011). Many of the C-N containing compounds in the products of these reactions are yet to be identified (Galloway et al. 2009). The formation of 1H-imidazole-2-carboxaldehyde from the reaction of ammonia and glyoxal by the general Debus mechanism is described by Galloway et al. (2009). This study is limited to the carbon K-edge, and further studies at the nitrogen and oxygen edges may provide more insight into the functional group composition of these SOA product particles.

Table 3 shows the peak area of five functional groups normalized by total carbon based on the fitting of Gaussian peaks with a fixed full width at half maximum of 1 eV (Takahama et al. 2007; Takahama et al. 2010). Particles formed from glyoxal uptake experiments with $MgSO_4$+H_2SO_4 seeds exhibit larger peak areas of ketonic carbonyl as compared to those in the presence of NH_4HSO_4 seeds. The ketonic carbonyl group in $MgSO_4$+H_2SO_4 seeds is consistent with acid-catalyzed acetal formation. Alcohol peaks are particularly prominent in the experiments with acidic conditions (Figure 1), which may also indicate acid-catalyzed hydration (Jang et al. 2002).

Differences in STXM-NEXAFS spectra among the different seed types shows that the inorganic seed composition influences the functional group composition, likely because these inorganic ions act as catalysts for heterogeneous reactions of glyoxal (Nozière et al. 2009; Yu et

al. 2011). Previous studies (Volkamer et al. 2009; Galloway et al. 2011) have also shown the effect of seed aerosol composition on SOA formation from glyoxal.

3.1.2 Photooxidation (α-pinene, isoprene, 1,2,4-trimethylbenzene, and d-limonene)

Carbonyl and alkyl groups were the most important functional groups in SOA particles formed from α-pinene photooxidation (Table 3 and Figure 1). The ketonic carbonyl group peak area exceeded the carboxylic carbonyl group peak area for these particles. The spectra obtained from the particles formed from α-pinene had strong signals from the black carbon (BC) used as seeds, as shown by peaks at ~285 eV and ~291 eV, similar to those found in spectra from soot particles (Braun et al. 2005). Chamber studies have shown with a variety of analytical techniques that the SOA products from α-pinene photooxidation contain ketonic and carboxylic groups (as summarized in Table 2 of Schwartz et al. 2010). The STXM-NEXAFS spectra in this study are consistent with these results as they also show strong absorption from these groups in SOA single particles formed from photooxidation of α-pinene.

We quantified the distribution of chemical components in particles formed from the photooxidation of α-pinene in the presence of BC seeds. We also studied variations in absorbance of the aromatic peak (at 285 eV) as a function of particle radius according to the procedures described by Takahama et al. (2010). Detailed procedures and results are given in the supplementary information. The particle core size was not detectable using a nonlinear squares fitting of a layered model (assuming a linear combination of BC and SOA, as described in Takahama et al. 2010). The outer layer of the particles contains high aromaticity. Results suggest that α-pinene SOA and BC are not segregated into a core-shell morphology within the

mixed particle (BC + α-pinene SOA). Particles with similar peak structure in the particle-averaged spectra but without such core-shell morphology have been observed in Pasadena, California, during the CalNex field campaign (Thompson et al. 2012; Hayes et al. 2012-in review).

In contrast to the particles formed exclusively from α-pinene, SOA from mixtures of α-pinene and isoprene contained fewer ketonic carbonyl and more carboxylic carbonyl, alkyl, and organic hydroxyl groups based on peak areas (Table 3). The ratio of ketonic to carboxylic group (peak area) was twice as large in the α-pinene experiments without isoprene compared to those with isoprene. The SOA formed from α-pinene and isoprene exhibit larger peak areas of hydroxyl group compared to that from only α-pinene. The SOA formed from isoprene photooxidation contain compounds such as C_5-alkene triols, 2-methyltetrols and its derivatives, carboxylic acids, epoxydiols and dimers that are enriched with hydroxy and carbonyl functional groups (Claeys et al. 2004; Surratt et al. 2006). Most of the above SOA products identified from isoprene photooxidation contain organic hydroxyl and alkyl groups (Schwartz et al. 2010). None of the identified SOA constituents (from isoprene) contain the ketonic carbonyl group, with the exception of the methylglyoxal sulfate isomer. This is consistent with the lower ketonic carbonyl peak area for the SOA formed from both α-pinene and isoprene. Glyoxal, a product of isoprene oxidation, may also cause the increase in carboxylic carbonyl and alkyl group, as described in section 3.1.1.

SOA formed from 1,2,4-TMB contains a larger contribution from carboxylic carbonyl, alkyl, and alcohol groups compared to ketonic carbonyl and aromatic groups (Table 3 and Figure 1). Measurements from FTIR spectroscopy in the same experiment showed the particles to be

composed of alcohol, organic nitrate, alkane, and carbonyl groups (Liu et al. 2012a). The aromatic (or alkene) group contribution had the smallest peak area of the functional groups for the measured spectra from the 1,2,4-TMB SOA experiments (see Table 3). TMB oxidation products in the particle phase contain low aromatic content (<5-10%) because TMB oxidation resulting in OH-TMB adducts follows the reaction with O_2 leading to the predominance of ring-opened products (Holes et al. 1997). Pathways for ring-retaining products also depend on the NO_x level, and ring-opening products are expected to be formed in high-NO_x conditions (Kautzman et al. 2010). The laboratory experiments with 1,2,4-TMB were conducted in a high NO_x-regime. The SOA formed from 1,3,5-TMB contains one hydroxyl and three carbonyl groups per average molecule (Holes et al. 1997). In comparison, the mean ratio (peak area) of carbonyl groups to hydroxyl groups in SOA from 1,2,4-TMB was 2.4 (Table 3). The SOA from 1,2,4-TMB photooxidation includes compounds like benzoquinones, benzaldehydes, benzoic acids, dimethylphenols, dimethylfurandione, furanones, glyoxal, and methylglyoxal (Forstner et al. 1997; Yu et al. 1997).

The STXM-NEXAFS spectra of particles formed from d-limonene photooxidation showed distinctive sharp peaks in the alkyl and carboxylic carbonyl group regions (Figure 1). The experiments for d-limonene were performed without any seed aerosols and did not show strong aromatic or alkene absorbance. Previous studies of compounds formed from d-limonene oxidation included ring-opening products that consist of alkyl, carboxylic acid, aldehyde, and alcohol functional groups (Glasius et al. 2000; Jaoui et al. 2006). Accordingly the organic functional groups identified by STXM-NEXAFS spectral are consistent with molecules

identified in d-limonene photooxidation, but the limited resolution of the single-particle approach prevents quantitative findings.

3.2 Morphology and size-dependence

Most of the particles identified by STXM from chamber experiments had smooth, circular 2-dimensional shapes, except for those produced from 1,2,4-TMB and d-limonene. The characteristic particle shapes and distributions of functional groups within particles are illustrated in Figure 2. The abundance of functional groups shown in Figure 2 was determined within each particle by peak-fitting individual NEXAFS spectra for each pixel, according to the criteria outlined by Takahama et al. (2010). The aspect ratios, i.e. the ratios of the length of the maximum to the minimum axes (Takahama et al. 2010), of the particles from glyoxal uptake experiments were less than or equal to 1.2, indicating nearly circular two-dimensional shapes after impaction on the Si_3N_4 windows. All particles from the glyoxal uptake experiments had smaller aspect ratios compared to photooxidation experiments (Table 3). Most of the particles formed from d-limonene photooxidation were irregular (aspect ratio: 1.58 ± 0.55). Many particles formed from 1,2,4-TMB and d-limonene laboratory chamber experiments without seed aerosols were non-spherical. In fact, the largest aspect ratios were observed for these two SOA precursors. However, particle shapes measured by microscopy may be altered by impaction, in particular for supermicron particles, so the implications of these results for the shapes of atmospheric particles are not clear.

There was no trend between the particle size and functional groups among the chamber particles, suggesting that most of the functional groups were distributed uniformly with size

(Tivanski et al. 2007). A statistical test of the chemical heterogeneity (Takahama et al. 2010) by cluster analysis of the pixel regions of the single particles did not show differences among the spectra of the clusters regardless of the experiment type.

3.3 Comparison of chamber with ambient particles

A total of 114 particles (out of 338 particles) collected from several field campaigns showed STXM-NEXAFS spectra similar to particles formed from the various SOA precursors inside the laboratory chambers. Figure 3 illustrates the spectra of selected ambient particles along with similar spectra from chamber SOA with differenent precursors. Spectra similar to those formed from α-pinene mixed with isoprene and from 1,2,4-TMB were the ones that were most frequently found to be similar to spectra from ambient particles. Quantitative comparisons of spectra from ambient and chamber particles were made using the cosine angle (or "dot product") metric given in Eqn. (1) (in which larger cosine angle metrics indicate better matches). Additional spectroscopic similarities were identified by visual comparison of peaks in overlaid spectra. The quantitative cosine angle metrics from the comparison of ambient particles with all the chamber particles from different SOA precursors are shown in Figure 4. Selected ambient particles with at least two matching peaks are illustrated with dark circles in Figure 4; spectra of these comparisons are illustrated in Figure 3 and the details are given in Table 2.

All ambient and chamber particles showed absorbance for alkyl groups (290.8-293 eV) and carboxylic carbonyl groups (288.2-288.9 eV) (green and light blue shaded area in Figure 3). Atmospheric particles (Figure 3a) collected from Scripps Pier, Whistler (2008 and 2010), MILAGRO, and VOCALS had similar spectral characteristics with SOA formed from glyoxal

uptake experiments ($NaNO_3$ seeds), namely they had peaks present at both ~288.7 and ~290.8 eV.

Ambient particles (Figure 3b) with similar features to 1,2,4-TMB had matching peaks at ~288.5, ~290.5, and ~297.38 eV (last peak not shown in the figure). These ambient particles also had a peak around ~285 eV for black carbon as combustion is the main source of 1,2,4-TMB. Measurement campaigns from Bakersfield, Whistler (2008), Scripps Pier, MILAGRO, and VOCALS had particles similar to the SOA particles formed from 1,2,4-TMB. Additionally, three particles shown by Takahama et al. (2007) as particle-type 'a' ("secondary") also showed similar spectral features with particles formed from 1,2,4-TMB. The type 'a' spectra were the SOA particles with characteristic carboxylic group absorbance, and these particle types were very commonly observed at field campaigns (Takahama et al., 2007). The main particle type at MILAGRO, analyzed from positive matrix factorization of STXM-NEXAFS spectra, were soot-like, secondary, and biomass burning (Liu et al. 2009). The spectral similarities of STXM-NEXAFS for particles from MILAGRO with chamber particles provide additional evidence that those particles consisted primarily of secondary components and suggest that α-pinene and 1,2,4-TMB may have been similar to the precursors that formed the secondary components. Scripps Pier particles had large carboxylic acid groups associated with combustion sources and were formed mainly from ozone-driven processes (Liu et al. 2011). Many Scripps Pier particles had spectral features similar to the particles formed from 1,2,4-TMB in the chamber experiments. This is consistent with FTIR spectroscopy and aerosol mass spectrometry measurements that showed organic aerosols during the sampling period were strongly influenced by urban emissions from Los Angeles (Liu et al. 2011). Sources of organic aerosols during the

VOCALS campaign were mainly continental anthropogenic emissions, and about 73% of total organic aerosol mass was contributed by carboxylic acid and alkane functional groups (Hawkins et al. 2010). Particles during the CalNex campaign at Bakersfield were largely organic and primarily originated from vehicular fossil fuel sources (Ahlm et al. 2012b; Liu et al., 2012b).

Particles (Figure 3c and d) similar to those formed from α-pinene (with and without isoprene) photooxidation were observed at MILAGRO, Whistler (2008 and 2010), and Scripps Pier. Ambient particles similar to α-pinene and isoprene had similar peaks at 288.5 and 290.5 eV while those similar to SOA from only α-pinene had similar peaks at 288.5 and 292 eV. The SOA experiments for α-pinene (with and without isoprene) were performed with BC seeds, and thus there is also a peak at ~285.5 eV in these spectra. The quantitative comparison by the cosine angle metric is strongly influenced by the absorption of the BC seed particles, making the interpretation of the similarities and differences problematic. Thus, the ambient particles with similar spectral characteristics as BC+NH_4HSO_4+α-pinene SOA represent the similarity with particles containing a mixture of BC and α-pinene SOA, and not necessarily to pure α-pinene SOA. Details on mixing of these particles are given in the supplementary information. As the BC+α-pinene SOA particles did not appear to be spatially separated with respect to their graphitic and organic constituents (supplementary information), subtraction and statistical techniques were unable to isolate the pure SOA spectra in these mixed particles. However, we find that BC+α-pinene SOA spectra indicated enrichment with respect to carboxylic and alkyl functional groups, consistent with the SOA products identified in previous α-pinene oxidation experiments (Hatakeyama et al. 1989; Yu et al. 1998). Consequently, the particles identified as being spectrally similar are matched on the similarity to the absorption peaks of these two

carboxylic and alkyl functional groups. Previous studies at Whistler during 2008 and 2010 indicated that SOA formation was likely largely from biogenic emissions from α-pinene-emitting pine tree forests (Schwartz et al. 2010; Pierce et al. 2012; Ahlm et al. 2012a). Particles analyzed by STXM from Whistler (2010) were collected during a period with high monoterpene and isoprene mixing ratios, and positive matrix factorization analysis of organic functional group concentrations measured by FTIR spectroscopy also showed that biogenic compounds were the main source of SOA during that period (Ahlm et al. 2012a). Whistler (2010) with SOA precursors except d-limonene had lower cosine angle metric than Whistler (2008) (Figure 8). Recently, pinene oxidation products, such as highly oxidized multifunctional molecules (with high molecular weight) observed in chamber experiments, have also been identified in ambient air at a boreal forest site in Hyytiälä, Finland (Ehn et al. 2012). Terpenoid acids (e.g. pinic and limonic acids) formed from SOA precursors such as α-pinene and d-limonene are also reported in fine aerosols from K-puszta, Hungary (Yasmeen et al. 2011).

Particles (Figure 3e) similar to the SOA formed from d-limonene were observed during VOCALS, Bakersfield, and Whistler (2010). Compared to particles produced from other SOA precursors, those produced from d-limonene were similar to fewer ambient particles. However, the particles that did match were quite similar, with three common peaks at ~287.6, 288.7, and 290.5 eV (corresponding to the functional groups alkyl and carboxylic carbonyl). These groups are consistent with the composition of many d-limonene photooxidation chamber products that have been identified, including limonic acids, limonaldehydes, hydroxylimononic acids (Jaoui et al., 2006). The strong match to the d-limonene particles suggests that the organic fraction of particles in these studies were largely biogenic SOA. Limonene is emitted by both natural (trees,

vegetation), and anthropogenic sources (agriculturally grown plants, household products) (Iinuma et al., 2007 and references therein). The results here provide evidence that ambient particles may contain SOA from d-limonene or similar precursors at both urban and rural sites.

4. Conclusions

The functional group composition of particles generated in chamber experiments (both dark and light conditions) from five SOA precursors were analyzed by STXM-NEXAFS spectroscopy, and these chamber-generated particles were compared with ambient particles collected from six field campaigns. Individual particles in chamber experiments showed carboxylic carbonyl and five other functional groups. All five measured functional groups were fairly uniformly distributed across the entire area of the particles analyzed. The chamber particles formed from glyoxal uptake displayed spectral differences associated with the type of inorganic aerosol seed used. SOA functionalities such as carbon-nitrogen containing groups were present mainly in particles formed on ammonium bisulfate seeds, and carboxylic carbonyl groups had stronger signals in particles formed on sodium sulfate seeds. The observed functional groups are consistent with the reaction products of carbon-nitrogen containing compounds, acids, and various oligomers reported in previous glyoxal uptake studies. These reaction products are similar to those identified in bulk filter particle analysis by other studies (Galloway et al. 2009; Yu et al. 2011). Particles formed from photooxidation of α-pinene, α-pinene with isoprene, and d-limonene had stronger absorption in the regions of carbonyl and alkyl groups relative to the alcohol and amine functional groups.

The measured STXM-NEXAFS functional group compositions are consistent with previous experiments. SOA formation is one of the main aerosol sources in the atmosphere, and chamber experiments are often performed to simulate and understand ambient atmospheric chemical mechanisms. In this work, we investigated ambient organic aerosol composition and potential SOA precursors by comparing the STXM-NEXAFS spectra of SOA from chamber studies with the spectra of ambient particles, of which 114 particles (out of 338) showed similarities tested by the cosine angle metric exceeding 0.9. Peaks at the carboxylic and alkyl group absorbance regions were found in all 114 ambient particles. Particles from the SOA precursors glyoxal ($NaNO_3$ seeds), α-pinene with isoprene (BC and NH_4HSO_4 seeds), and 1,2,4-TMB represented most of the ambient particles. Among the chamber SOA precursors used for the comparison, more particles similar to SOA from 1,2,4-TMB, a precursor of anthropogenic origin, were found at sites with urban anthropogenic influence such as Bakersfield and Scripps Pier, while particles resembling SOA from biogenic precursors, such as α-pinene and isoprene, were more commonly observed at remote sites such as Whistler, British Columbia.

References

Ahlm, L., Shakya, K.M., Russell, L.M., Schroder, J., Wong, J.P.S., Cziczo, D.J., Sjostedt, S., Hayden, K., Liggio, J., Wentzell, J., Wiebe, H.A., Mihele, C., Leaitch, W.R., and Macdonald, A.M. (2012a). Temperature-dependent accumulation mode particle and cloud nuclei concentrations from biogenic sources during WACS 2010. *Atmos. Chem. Phys.Discuss.* 12, 27989-28031.

Ahlm, L., Liu, S., Day, D.A., Russell, L.M., Weber, R., Gentner, D.R., Goldstein, A.H., DiGangi, J.P., Henry, S.B., Keutsch, F.N., VandenBoer, T.C., Markovic, M.Z., Murphy, J.G., Ren, X., and Scheller, S. (2012b). Formation and growth of ultrafine particles from secondary sources in Bakersfield, California. *J. Geophys. Res.* 117, D00V08, doi: 10.1029/2011JD017144.

Braun, A. (2005). Carbon speciation in airborne particulate matter with C (1S) NEXAFS spectroscopy. *J. Environ. Monit.* 7:1059-1065.

Claeys, M., Graham, B., Vas, G., Wang, W., Vermeylen, R., Pashynska, V., Cafmeyer, J., Cuyon, P., Andreae, M.O., Artaxo, P., and Maenhaut, W. (2004). Formation of secondary organic aerosols through photooxidation of isoprene. *Science* 303:1173-1176.

Chhabra, P.S., Flagan, R.C., and Seinfeld, J.H. (2010). Elemental analysis of chamber organic aerosol using an aerodyne high-resolution aerosol mass spectrometer. *Atmos. Chem. Phys.* 10, 4111-4131.

Cody, G.D., Ade, H., Alexander, C.M.O., Araki, T., Butterworth, A., Fleckenstein, H., Flynn, G., Gilles, M.K., Jacobsen, C., Kilcoyne, A.L.D., Messenger, K., Sandford, S.A., Tyliszczak, T., Westphal, A.J., Wirick, S., and Yabuta, H. (2008). Quantitative organic and light element analysis of Comet 81P/Wild 2 particles using C-, N-, and O-μ-XANES. *Met. Planet. Sci.* 43, 353-365.

De Haan, D.O., Corrigan, A.L., Smith, K.W., Stroik, D.R., Turley, J.J., Lee, F.E., Tolbert, M.A., Jimenez, J.L., Cordova, K.E., and Ferrell, G.R. (2009). Secondary organic aerosol-forming reactions of glyoxal with amino acids. *Environ. Sci. Technol*. 43(8), 2818-2824.

Day, D.A., Takahama, S., Gilardoni, S., and Russell, L.M. (2009). Organic composition of single and submicron particles in different regions of western North America and the eastern Pacific during INTEX-B 2006. *Atmos. Chem. Phys.* 9:5433-5446.

Ehn, M., Kleist, E., Junninen, Petäjä, T., Lönn, G., Schobesberger, S., Maso, M.D., Trimborn, A., Kulmala, M., Worsnop, D.R., Wahner, A., Wildt, J., and Mentel, T.F. (2012). Gas phase formation of extremely oxidized pinene reaction products in chamber and ambient air. *Atmos. Chem. Phys*. 12, 5113-5127.

Ervens, B., Turpin, B.J., and Weber, R.J. (2011). Secondary organic aerosol formation in cloud droplets and aqueous particles (aqSOA): a review of laboratory, field and model studies. *Atmos. Chem. Phys*. 11: 11069-11102.

Forstner, H.J.L., Flagan, R.C., and Seinfeld, J.H. (1997). Secondary organic aerosol from the photooxidation of aromatic hydrocarbons: Molecular composition. *Environ. Sci. Technol.* 31:1345-1358.

Fu, T.-M., Jacob, D.J., Wittrock, F., Burrows, J.P., Vrekoussis, M., and Henze, D.K. (2008). Global budgets of atmospheric glyoxal and methylglyoxal and implications for formation of secondary organic aerosols. *J. Geophys. Res.* 113, D15303, doi:10.1029/2007JD009505.

Galloway, M.M., Chhabra, P.S., Chan, A.W.H., Surratt, J.D., Flagan, R.C., Seinfeld, J.H., and Keutsch, F.N. (2009). Glyoxal uptake on ammonium sulphate seed aerosol: Reaction products and reversibility of uptake under dark and irradiated conditions. *Atmos. Chem. Phys.* 9:3331-3345.

Galloway, M.M., Loza, C.L., Chhabra, P.S., Chan, A.W.H., Yee, L.D., Seinfeld, J.H., and Keutsch, F.N. (2011). Analysis of photochemical and dark glyoxal uptake: Implications for SOA formation. *Geophys. Res. Lett.* 38, L17811, doi:10.1029/2011GL048514.

Glasius, M., Lahaniati, M., Calogirou, A., Bella, D.D., Jensen, N.R., Hjorth, J., Kotzias, D., and Larsen, B.R. (2000). Carboxylic acids in secondary aerosols from oxidation of cyclic monoterpenes by ozone. *Environ. Sci. Technol.* 34:1001-1010.

Griffin, R.J., Cocker, D. R., Seinfeld, J.H., and Dabdub, D. (1999). Estimate of global atmospheric organic aerosol from oxidation of biogenic hydrocarbons. *Geophys. Res. Lett.* 26:2721-2724.

Hatakeyama, S., Izumi, K., Fukuyama, T., and Akimoto, H. (1989). Reactions of ozone with alpha-pinene and beta-pinene in air: Yields of gaseous and particulate products. *J. Geophys. Res*. 94:13013-13024.

Hawkins, L.N. and Russell, L.M. (2010). Polysaccharides, proteins, and phytoplankton fragments: Four chemically distinct types of marine primary organic aerosol classified by single particle spectromicroscopy. *Adv. Meteorol.* doi:10.1155/2010/612132.

Hawkins, L.N., Russell, L.M., Covert, D.S., Quinn, P.K., and Bates, T.S. (2010). Carboxylic acids, sulfates, and organosulfates in processed continental organic aerosol over the southeast Pacific Ocean during VOCALS-REx 2008. *J. Geophys. Res.* 115, D13201, doi:10.1029/2009JD013276.

Hayes, P.L., Ortegal, A.M., Cubison, M.J., Froyd, K.D., Zhao, Y., Cliff, S.S., Hul, W.W, Toohey, D.W., Flynn, J.H., Lefer, B.L., Grossberg, N., Alvarez, S., Rappenglück, B., Taylor, W., Allan, J.D., Holloway, J.S., Gilman, J.B., Kuster, W.C., Gouw, J.A., Massoli,

P., Zhang, X., Liu, J., Weber, R.J., Corrigan, A.L., Russell, L.M., Isaacman, G., Worton, D.R., Kreisberg, N.M., Hering, S.V., Goldstein, A.H., Thalman, R., Waxman, E.M., Volkamer, R., Lin, Y.H., Surratt, J.D., Kleindienst, T.E., Offenberg, J.H., Dusanter, S., Griffith, S., Stevens, P.S., Brioude, J., Angevine, W.M., and Jimenez, J.L. (2012). Aerosol Composition and Sources in Los Angeles during the 2010 CalNex Campaign. Submitted to *J. Geophys. Res.*

Henze, D.K. and Seinfeld, J.H. (2006). Global secondary organic aerosol from isoprene oxidation. *Geophys. Res. Lett.* 33, L09812, doi:10.1029/2006GL025976.

Hitchcock, A. aXis 2000. Available at http://unicorn.mcmaster.ca/aXis2000.html

Holes, A., Eusebi, A., Grosjean, D., and Allen, D.T. (1997). FTIR analysis of aerosol formed in the photooxidation of 1,3,5-Trimethylbenzene. *Aer. Sci. Technol.* 26:516-526.

Huisman, A.J., Hottle, J.R., Galloway, M.M., DiGangi, J.P, Coens, K.L., Choi, W., Faloona, I.C., Gilman, J.B., Kuster, W.C., Gouw, J., Brown, N.C.B., Goldstein, A.H., LaFranchi, B.W., Cohen, R.C., Wolfe, G.M., Thornton, J.A., Docherty, K.S., Farmer, D.K., Cubison, M.J., Jimenez, J.L., Mao, J., Brune, W.H., and Keutsch, F.N. (2011). Photochemical modeling of glyoxal at a rural site: observations and analysis from BEARPEX 2007. *Atmos. Chem. Phys*. 11, 8883-8897.

Iinuma, Y., Müller, C., Böge, O., Gnauk, T., and Herrmann, H. (2007). The formation of organic sulfate esters in the limonene ozonolysis secondary organic aerosol (SOA) under acidic conditions. *Atmos. Environ.* 41:5571-5583.

Jaoui, M., Corse, E., Kleindienst, T.E., Offenberg, J.H., Lewandowski, and Edney, E.O. (2006). Analysis of secondary organic aerosol compounds from the photooxidation of d-limonene

in the presence of NO_x and their detection in ambient $PM_{2.5}$. *Environ. Sci. Technol.* 40:3819-3828.

Jang, M. and Kamens, R.M. (2001). Characterization of secondary aerosol from the photooxidation of toluene in the presence of NO_x and 1-propene. *Environ. Sci. Technol.* 35:3626-3639.

Jang, M., Czoschke, N.M., Lee, S., and Kamens, R. (2002). Heterogeneous atmospheric aerosol production by acid-catalyzed particle-phase reactions. *Science* 298, 814-817.

Kanakidou, M., Seinfeld, J.H., Pandis, S.N., Barnes, I., Dentener, F.J., Facchini, M.C., Van Dingenen, R., Ervens, B., Nenes, A., Nielsen, C.J., Swietlicki, E., Putaud, J.P., Balkanski, Y., Fuzzi, S., Horth, J., Moortgat, G.K., Winterhalter, R., Myhre, C.E.L., Tsigaridis, K., Vignati, E., Stephanou, E.G., and Wilson, J. (2005). Organic aerosol and global climate modeling: a review. *Atmos. Chem. Phys.* 5:1053-1123.

Kautzman, K.E., Surratt, J.D., Chan, M.N., Chan, A.W.H., Hersey, S.P., Chhabra, P.S., Dalleska, N.F., Wennberg, P.O., Flagan, R.C., and Seinfeld, J.H. (2010). Chemical composition of gas- and aerosol-phase products from the photooxidation of naphthalene. *J. Phys. Chem. A* 114:913-934.

Kroll, J.H. and Seinfeld, J.H. (2008). Chemistry of secondary organic aerosol: Formation and evolution of low-volatility organics in the atmosphere. *Atmos. Environ.* 42:3593-3624.

Liu, S., Takahama, S., Russell, L.M., Gilardoni, S., and Baumgardner, D. (2009). Oxygenated organic functional groups and their sources in single and submicron organic particles in MILAGRO 2006 campaign. *Atmos. Chem. Phys.* 9:6849-6863.

Liu, S., Day, D.A., Shields, J.E., and Russell, L.M. (2011). Ozone-driven daytime formation of secondary organic aerosol containing carboxylic acid groups and alkane groups. *Atmos. Chem. Phys.* 11:8321-8341.

Liu, S., Shilling, J.E., Song, C., Hiranuma, N., Zaveri, A.Z., and Russell, L.M. (2012a). Hydrolysis of organonitrate functional groups in aerosol particles. *Aerosol Sci. Technol.* In press.

Liu, S., Ahlm, L., Day, D. A., Russell, L. M., Zhao, Y., Gentner, D. R., Weber, R. J., Goldstein, A. H., Jaoui, M., Offenberg, J. H., Kleindienst, T. E., Rubitschun, C., Surratt, J. D, Sheesley, R. J., and Scheller, S. (2012b). Secondary organic aerosol formation from fossil fuel sources contribute majority of summertime organic mass at Bakersfield. *J. Geophys. Res.* 117, D00V26, doi:10.1029/2012JD018170.

Liggio, J., Li, S.-M., and Mclaren, R. (2005). Heterogeneous reactions of glyoxal on particulate matter: Identification of acetals and sulfate esters. *Environ. Sci. Technol.* 39:1532-1541.

Madrid, H.J.C., Presto, A.A., and Donahue, N.M. (2010). Functionalization *vs.* fragmentation: n-aldehyde oxidation mechanisms and secondary organic aerosol formation. *Phys. Chem. Chem. Phys*. 12: 13975-13982.

Myneni, S.C.B. (2002). Soft X-ray spectroscopy and spectromicroscopy studies of organic molecules in the environment. *Rev. Min. Geochem*. 49, 485-579.

Ng, N.L., Kroll, J.H., Keywood, M.D., Bahreini, R., Varutbangkul, V., Flagan, R.C., Seinfeld, J.H., Lee, A., and Goldstein, A.H. (2006). Contribution of first- versus second-generation products to secondary organic aerosols formed in the oxidation of biogenic hydrocarbons. *Environ. Sci. Technol.* 40:2283-2297.

Nozière, B., Dziedzic, P., and Córdova, A. (2009). Products and kinetics of the liquid-phase reaction of glyoxal catalyzed by ammonium ions (NH_4^+). *J. Phys. Chem. A* 113:231-237.

Paulsen, D., Dommen, J., Kalberer, M., Prévôt, A.S.H., Richter, R., Sax, M., Steinhacher, M., Weingartner, E., and Baltensperger, U. (2005). Secondary organic aerosol formation by irradiation of 1,3,5-trimethylbenzene-NO_x-H_2O in a new reaction chamber for atmospheric chemistry and physics. *Environ. Sci. Technol*. 39, 2668-2678.

Pfaffenberger, L., Barmet, P., Slowik, J.G., Praplan, A.P., Dommen, J., Prévôt, A.S.H., Baltensperger, U. (2012). The link between organic aerosol mass loading and degree of oxygenation: an α-pinene photooxidation study. *Atmos. Chem. Phys. Discuss*. 12, 24735-24764.

Pierce, J.R., Leaitch, W.R., Liggio, J., Westervelt, D.M., Wainwright, C.D., Abbatt, J.P.D., Ahlm, L., Al-Basheer, W., Cziczo, D.J., Hayden, K.L., Lee, A.K.Y., Li, S.,M., Russell, L.M., Sjostedt, S.J., Strawbridge, K.B., Travis, M., Vlasenko, A., Wentzell, J.J.B., Wiebe, H.A., Wong, J.P.S., and Macdonald, A.M. (2012). Nucleation and condensational growth to CCN sizes during a sustained pristine biogenic SOA event in a forested mountain valley. *Atmos. Chem. Phys*. 12, 3147-3163.

Rühl, E., Wen, A.T., and Hitchcock, A.P. (1991). Inner-shell excitation of η^5-$C_5H_5Co(CO)_2$ and related compounds studied by gas phase electron energy loss spectroscopy. *J. Elect. Spectr. Rel. Phenom*. 57:137-164.

Russell, L.M., Maria, S.F., and Myneni, S.C.B. (2002). Mapping organic coatings on atmospheric particles. *Geophys. Res. Lett.* 29(16), 1779, doi:10.1029/2002GL014874.

Russell, L.M., Bahadur, R., and Ziemann, P.J. (2011). Identifying organic aerosol sources by comparing functional group composition in chamber and atmospheric particles. *P. Natl. Acad. Sci. USA* doi:10.1073/pnas.1006461108.

Schwartz, R.E., Russell, L.M., Sjostedt, S.J., Vlasenko, A., Slowik, J.G., Abbatt, J.P.D., Macdonald, A.M., Li, S.M., Liggio, J., Toom-Sauntry, D., and Leaitch, W.R. (2010). Biogenic oxidized organic functional groups in aerosol particles from a mountain forest site and their similarities to laboratory chamber products. *Atmos. Chem. Phys*. 10:5075-5088.

Solomon, D., Lehmann, J., Kinyangi, J., Liang, B., Hanley, K., Heymann, K., Wirick, S., and Jacobsen, C. (2009). Carbon (1s) NEXAFS spectroscopy of biogeochemically relevant organic reference compounds. *Soil Sci. Soc. Am. J.* 73:1817-1830.

Solomon, D., Lehmann, J., Harden, J., Wang, J., Kinyangi, J., Heymann, K., Karunakaran, C., Lu, Y., Wirick, S., and Jacobsen, C. (2012). Micro- and nano-environments of carbon sequestration: Multi-element STXM-NEXAFS spectromicroscopy assessment of microbial carbon and mineral associations. *Chem. Geol.* doi:10.1016/j.chemgeo.2012.02.002.

Surratt, J.D., Murphy, S.M., Kroll, J.H., Ng, N.L., Hildebrandt, L., Sorooshian, A., Szmigielski, R., Vermeylen, R., Maenhaut, W., Claeys, M., Flagan, R.C., and Seinfeld, J.H. (2006). Chemical composition of secondary organic aerosol formed from the photooxidation of isoprene. *J. Phys. Chem. A* 110:9665-9690.

Tabb, D.L., MacCoss, M.J., Wu, C.C., Anderson, S.D., and Yates III, J.R. (2003). Similarity among tandem mass spectra from proteomic experiments: Detection, significance, and utility. *Anal. Chem. A* 10.1021/ac026424.

Takahama, S., Gilardoni, S., Russell, L.M., and Kilcoyne, A.L.D. (2007). Classification of multiple types of organic carbon composition in atmospheric particles by scanning transmission X-ray microscopy analysis. *Atmos. Environ*. 41:9435-9451.

Takahama, S., Liu, S., and Russell, L.M. (2010). Coatings and clusters of carboxylic acids in carbon-containing atmospheric particles from spectromicroscopy and their implications for cloud-nucleating and optical properties. *J. Geophys. Res.* 115, D01202, doi:10.1029/2009JD012622, 2010.

Takahama, S., Schwartz, R.E., Russell, L.M., Macdonald, A.M., Sharma, S., and Leaitch, W.R. (2011). Organic functional groups in aerosol particles from burning and non-burning forest emissions at a high-elevation mountain site. *Atmos. Chem. Phys*. 11:6367-6386.

Thompson, J.E., Hayes, P., Jimenez, J.L., Adachi, K., Zhang, X., Liu, J., Weber, R.J., and Buseck, P.R. (2012). Aerosol optical properties at Pasadena, CA during CalNex 2010. *Atmos. Environ*. 55:190-200.

Tivanski, A.V., Hopkins, R.J., Tyliszczak, T., and Gilles, M.K. (2007). Oxygenated interface on biomass burn tar balls determined by single particle scanning transmission X-ray microscopy. *J. Phys. Chem. A* 111:5448-5458.

Volkamer, R., Martini, F.S., Molina, L.T., Salcedo, D., Jimenez, J.L., and Molina M.J. (2007). A missing sink for gas-phase glyoxal in Mexico City: formation of secondary organic aerosol. *Geophys. Res. Lett*. 34, L13805, doi:10.1029/2007g1030752.

Volkamer, R., Ziemann, P.J., and Molina, M.J. (2009). Secondary organic aerosol formation from acetylene (C_2H_2): seed effect on SOA yields due to organic photochemistry in the aerosol aqueous phase. *Atmos. Chem. Phys.* 9:1907-1928.

Washenfelder, R.A., Young, C.J., Brown, S.S., Angevine, W.M., Atlas, E.L., Blake, D.R., Bon, D.M., Cubison, M.J., de Gouw, J.A., Dusanter, S., Flynn, J., Gilman, J.B., Graus, M., Griffith, S., Grossberg, N., Hayes, P.L., Jimenez, J.L., Kuster, W.C., Lefer, B.L., Pollack, I.B., Ryerson, T.B., Stark, H., Stevens, P.S., and Trainer, M.K. (2011). The glyoxal budget and its contribution to organic aerosol for Los Angeles, California,during CalNex 2010. *J. Geophys. Res*. 116, D00V02, doi:10.1029/2011JD016314.

Yasmeen, F., Szmigielski, R., Vermeylen, R., González, Y.G., Surratt, J.D., Chan, A.W.H., Seinfeld, J.H., Maenhaut, W., and Claeys, M. (2011). Mass spectrometric characterization of isomeric terpenoic acids from the oxidation of α-pinene, β-pinene, d-limonene, and Δ^3-carene in fine forest aerosol. *J. Mass Spectrom*. 46, 425-442.

Yee, L.D., Craven, J.S., Loza, C.L., Schilling, K.A., Ng, N.L., Canagaratna, M.R., Ziemann, P.J., Flagan, R.C., and Seinfeld, J.H. (2012). Secondary organic aerosol formation from low-NO_x photooxidation of dodecane: Evolution of multigeneration gas-phase chemistry and aerosol composition. *J. Phys. Chem. A* 116, 6211-6230.

Yu, J., Jeffries, H., and Sexton, K.G. (1997). Atmospheric photooxidation of alkylbenzenes-I. Carbonyl product analyses. *Atmos. Environ*. 31:2261-2280.

Yu, J., Flagan, R., and Seinfeld, J.H. (1998). Identification of products containing –COOH, -OH, and –C=O in atmospheric oxidation of hydrocarbons. *Environ. Sci. Technol.* 32:2357-2370.

Yu, G., Bayer, A.R., Galloway, M.M., Korshavn, K.J., Fry, C.G., and Keutsch, F.N. (2011). Glyoxal in aqueous ammonium sulfate solutions: Products, kinetics and hydration effects. *Environ. Sci. Technol*. 45:6336-6342.

ACKNOWLEDGEMENTS

Support for this work was provided by the grant ATM-0904203 from National Science Foundation. Support for sampling at two of the smog chambers was provided by the European Commission FP7 project EUROCHAMP-2 and the Pacific Northwest National Laboratory's Aerosol Climate Initiative. STXM-NEXAFS spectra were acquired at beamline 5.3.2.2 at the ALS, which is supported by the Director of the Office of Science, Department of Energy, under Contract No. DE-AC02-05CH11231. We acknowledge John H. Seinfeld, Jill S. Craven, and Christine L. Loza from California Institute of Technology, W. Richard Leaitch from Environment Canada, and Ashley Corrigan, Amanda Frossard, and Lars Ahlm for their assistance with experiments and analyses discussed here.

Figure 1. Average STXM-NEXAFS spectra of SOA particles formed from the glyoxal uptake experiments with (a) ammonium bisulfate (NH_4HSO_4), (b) magnesium sulfate+sulfuric acid ($MgSO_4$+H_2SO_4), (c) sodium nitrate ($NaNO_3$), and (d) sodium sulfate (Na_2SO_4) seeds, from the photooxidation of (e) α-pinene with black carbon and NH_4HSO_4, (f) α-pinene and isoprene with black carbon and NH_4HSO_4, (g) 1,2,4-trimethylbenzene, and (h) d-limonene. The shaded regions show the absorbance region for the functional groups labeled on top axis. Y-axis represents

the optical density in arbitrary units that is normalized by the procedure given in section 2.3.

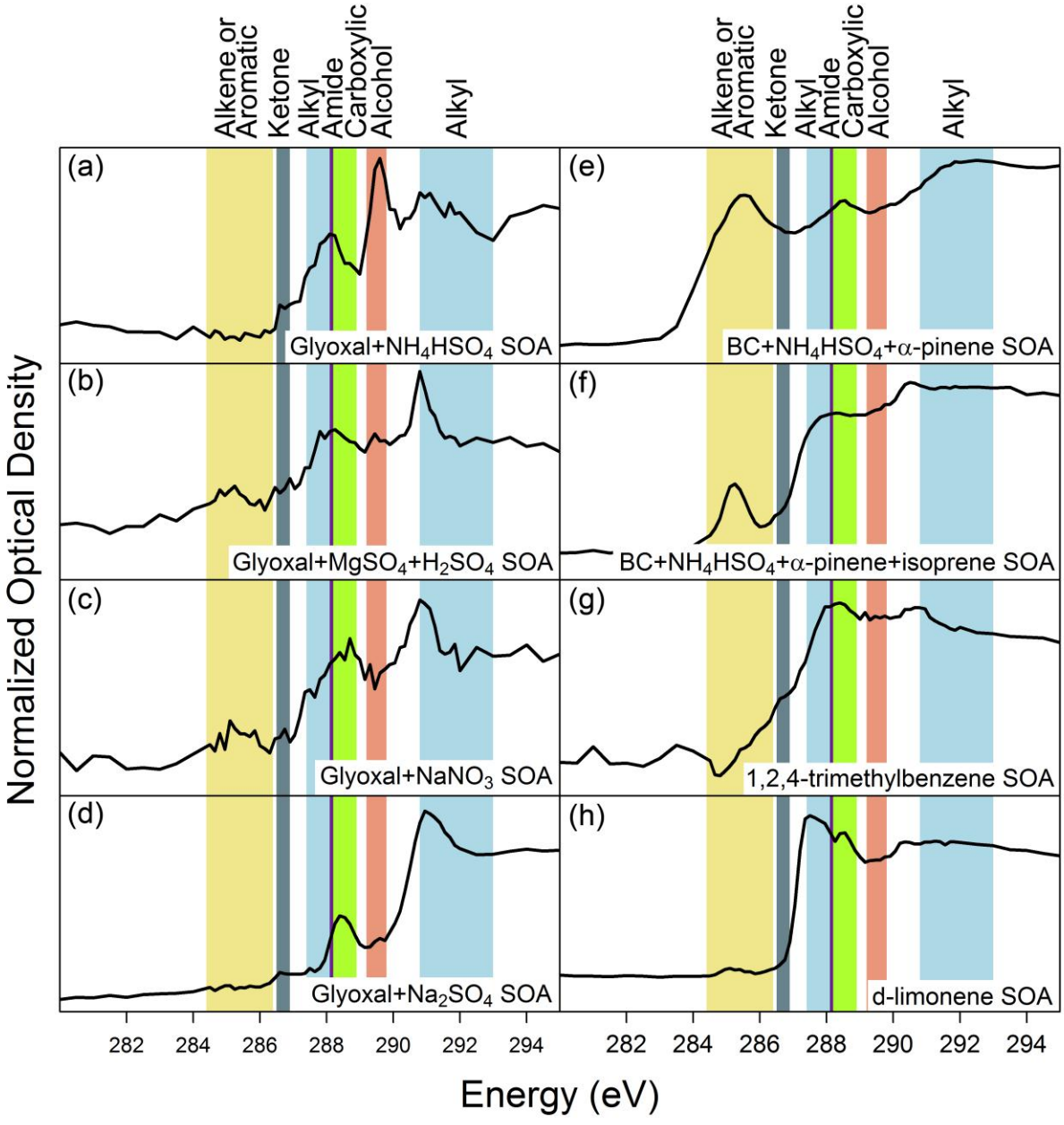

Figure 2. Spatial distribution of total carbon and functional groups within the SOA particles from the precursors in the following order: (a) glyoxal + NH_4HSO_4 seeds, (e) α-

pinene + BC + NH_4HSO_4, (f) α-pinene with isoprene + BC + NH_4HSO_4, (g) 1,2,4-trimethylbenzene, and (h) d-limonene. For each group, the relative concentrations of each functional group are shown from light to dark (in color from blue to red).

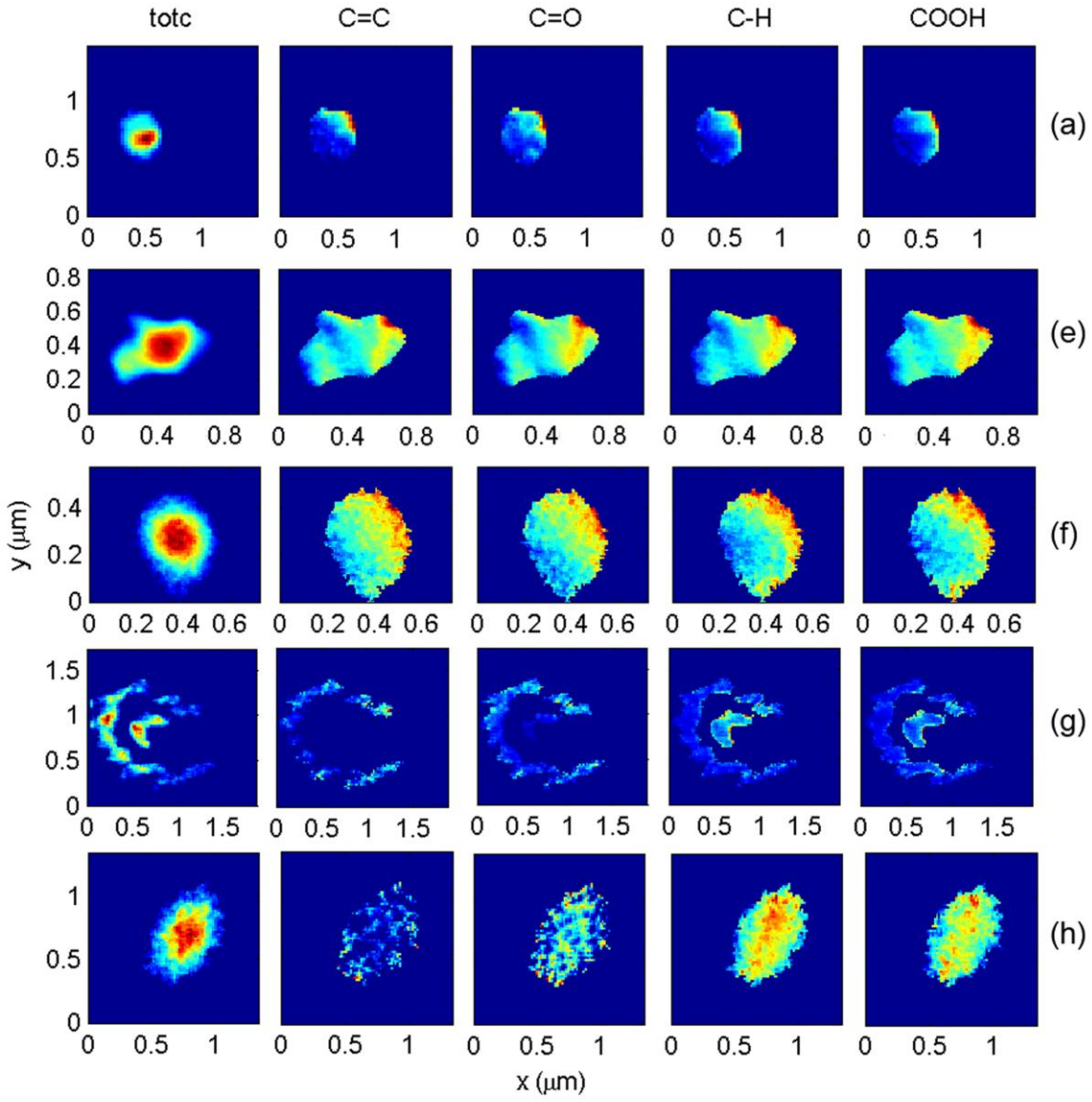

Figure 3. Comparison of SOA spectra formed from (a) glyoxal ($NaNO_3$ seeds), (b) 1,2,4-trimethylbenzene, (c) black carbon + α-pinene with isoprene + NH_4HSO_4, (d) black

carbon + α-pinene + NH_4HSO_4, and (e) d-limonene with ambient particles from Scripps Pier, Whistler (2008), Whistler (2010), Bakersfield (CalNex), VOCALS, and MILAGRO. Traces indicate the campaign location. The functional group regions are the same as those shown in Figure 1. Only selected spectra (all with cosine angle metric greater than 0.9) are shown here for the illustration; the complete list is given in Table 2. The wavelength range below and above 286 to 294 eV were not used for computing the cosine angle metric or for comparing peak similarities since they include signals that are not organic.

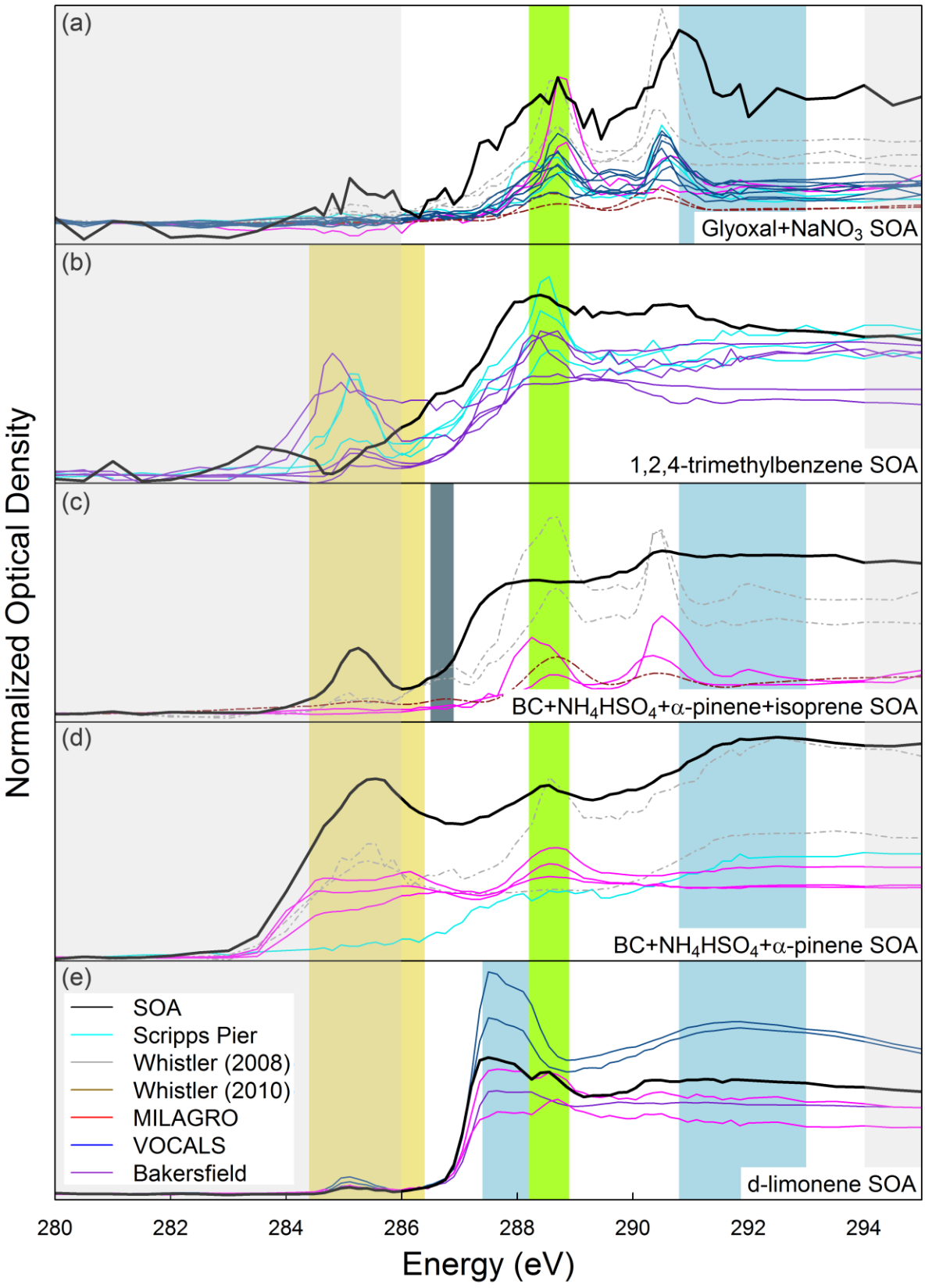

Figure 4. Calculated cosine angle metrics (from equation 1) for the comparisons of ambient particles from six field campaigns with SOA chamber particles formed from five different precursors with various seeds: glyoxal + NH_4HSO_4, glyoxal + $MgSO_4$ + H_2SO_4, glyoxal + $NaNO_3$, glyoxal + Na_2SO_4, black carbon + α-pinene + NH_4HSO_4, black carbon + α-pinene + isoprene + NH_4HSO_4, 1,2,4-trimethylbenzene (1,2,4-TMB), and d-limonene. Open circles are cosine angle metrics for all the comparisons, and dark circles are particles that had two or more similar peaks, as shown in Figure 3.

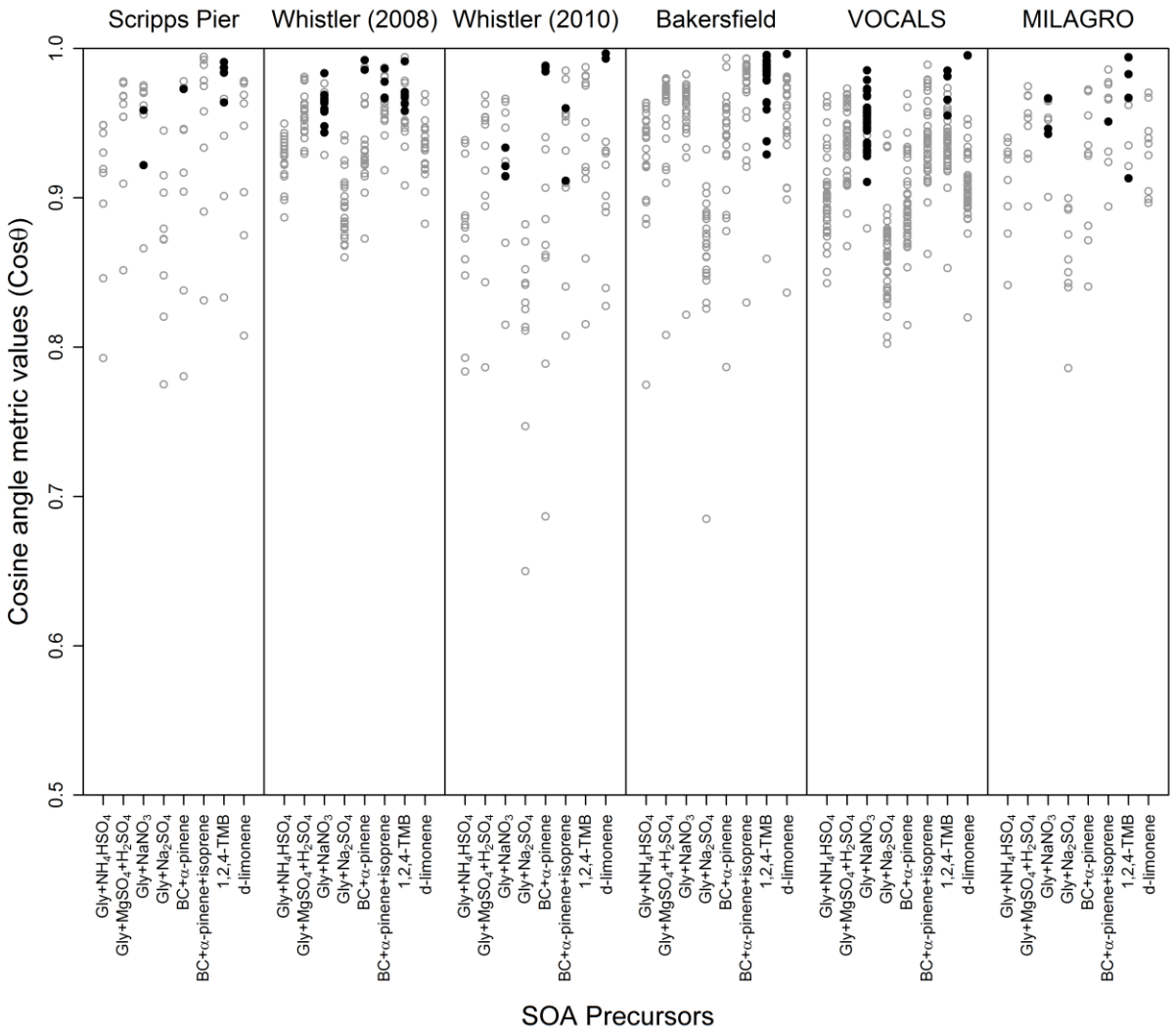

Table 1. Details of the experiments performed with various SOA precursors. The last column gives the total number of single particles analyzed at the Advanced Light Source (ALS).

Experiment	Date	Location	SOA precursor	Seed	RH (%)	Light	Number of particles (total: 75)

Glyoxal Uptake Experiments							
(a)	11/18/2009	Caltech	27 ppbv Glyoxal	Ammonium bisulfate	68	Off	3
(b)	11/17/2009	Caltech	33.5 ppbv Glyoxal	Magnesium sulfate + Sulfuric acid	80	Off	5
(c)	11/21/2009	Caltech	35 ppbv Glyoxal	Sodium nitrate	61	Off	3
(d)	11/20/2009	Caltech	38.5 ppbv Glyoxal	Sodium sulfate	79	Off	9
Photooxidation Experiments							
(e)	2/9/2011	PSI	45 ppbv α-pinene + 2-9 ppbv NO_x	Black Carbon (Tokai) + Ammonium bisulfate	28	On	21
(f)	2/11/2011	PSI	40 ppbv α-pinene + 400 ppbv Isoprene + 5-50 ppbv NO_x	Black Carbon (Tokai) + Ammonium bisulfate	70	On	13
(g)	3/15/2011	PNNL	300 ppbv 1,2,4-trimethylbenzene + 2000 ppbv HONO	No seeds	15-20	On	12
(h)	1/19/2012	UCLA	190 ppbv d-limonene + 290 ppbv NO_x	No seeds	24-39	On*	9

*Natural sunlight. RH: Relative humidity

Table 2. Total number of ambient samples from six field campaigns showing similar spectral characteristics (all with cosine angle metric greater than 0.9) with chamber SOA particles.

Field campaign	Location	Period	Number of	Similarity with	References

			particles (total: 114)	SOA precursor	
Megacity Initiative: Local and Global Research Observations (MILAGRO)	Urban and aircraft, Mexico (urban)	March 2006	9	Glyoxal uptake ($NaNO_3$ seeds); α-pinene and isoprene; 1,2,4-TMB	Liu et al. 2009
VAMOS Ocean-Cloud-Atmosphere-Land Study (VOCALS)	Southeast Pacific marine boundary layer (marine)	November 2008	41	Glyoxal uptake ($NaNO_3$ seeds); d-limonene; 1,2,4-TMB	Hawkins et al. 2010
Scripps Pier	La Jolla, San Diego, California (mixed sources)	August-September 2009	8	Glyoxal uptake ($NaNO_3$ seeds); α-pinene; α-pinene and isoprene; 1,2,4-TMB	Liu et al. 2011
Bakersfield (CalNex)	Bakersfield, California (urban)	May-June 2010	24	d-limonene; 1,2,4-TMB	Ahlm et al. 2012b; Liu et al. 2012b
Whistler (2008)	Whistler Peak, British Columbia (rural)	June 2008	22	Glyoxal uptake ($NaNO_3$ seeds); α-pinene; α-pinene and isoprene; 1,2,4-TMB	Schwartz et al. 2010
Whistler (2010)	Whistler Peak and Raven's Nest, British Columbia (rural)	July 2010	10	Glyoxal uptake ($NaNO_3$ seeds); α-pinene; α-pinene and isoprene; d-limonene	Pierce et al. 2012; Ahlm et al. 2012a

Table 3. Normalized peak area (by total carbon) of five functional groups based on the peak fitting (C=C at 285, C=O at 286.7, C-H at 287.7, COOH at 288.7, and COH at 289.5 eV). Aspect ratio of particles formed from the respective experiments is also given.

Experiments	Alkyl (C-H)	Aromatic (or Alkene) (C=C)	Ketonic carbonyl (C=O)	Carboxylic carbonyl (COOH)	Alcohol (COH)	Aspect ratio
<u>Glyoxal uptake</u>						
Ammonium bisulfate	1.25 ± 0.25	0.19 ± 0.17	0.23 ± 0.20	0.77 ± 0.38	1.62 ± 0.82	1.12 ± 0.05
Magnesium sulfate + Sulfuric acid	2.48 ± 1.09	0.83 ± 0.88	1.06 ± 0.89	2.36 ± 1.21	1.92 ± 1.71	1.16 ± 0.18
Sodium sulfate	0.32 ± 0.11	0.16 ± 0.12	0.31 ± 0.19	0.89 ± 0.27	0.04 ± 0.12	1.22 ± 0.10
<u>α-pinene</u>						
α-pinene + BC + NH_4HSO_4	0.83 ± 0.31	1.30 ± 0.54	1.06 ± 0.34	0.91 ± 0.31	0.56 ± 0.20	1.36 ± 0.31
α-pinene + isoprene + BC + NH_4HSO_4	1.22 ± 0.20	0.57 ± 0.26	0.37 ± 0.13	1.03 ± 0.16	0.76 ± 0.11	1.42 ± 0.19
1,2,4-trimethylbenzene	1.81 ± 0.29	0.16 ± 0.20	0.87 ± 0.34	1.89 ± 0.28	1.17 ± 0.12	1.61 ± 0.58
d-limonene	2.38 ± 0.35	0.07 ± 0.08	0.18 ± 0.09	1.49 ± 0.12	0.93 ± 0.07	1.58 ± 0.55

Mean and one standard deviation of values for the aspect ratio and normalized peak are shown in the table.

Supplemental Information for "Similarities in STXM-NEXAFS Spectra of Atmospheric Particles and Secondary Organic Aerosol generated from glyoxal, α-pinene, isoprene, 1,2,4-trimethylbenzene, and d-limonene"

Kabindra M. Shakya[1,2], Shang Liu[1], Satoshi Takahama[1,3], Lynn M. Russell[1]*, Frank N. Keutsch[4], Melissa M. Galloway[4,5], John E. Shilling[6], Naruki Hiranuma[6,7], Chen Song[6], Hwajin Kim[8], Suzanne E. Paulson[8], Lisa Pfaffenberger[9], Peter Barmet[9], Jay Slowik[9], André S. H. Prévôt[9], Josef Dommen[9], Urs Baltensperger[9]

[1]Scripps Institution of Oceanography, University of California, San Diego, La Jolla, California, USA
[2]Now at Division of Environmental Health, Department of Public Health, School of Public Health Sciences, University of Massachusetts, Amherst, Massachusetts, USA
[3]Now at École Polytechnique Fédérale de Lausanne (EPFL), Switzerland
[4]Department of Chemistry, University of Wisconsin-Madison, Madison, Wisconsin, USA
[5]Now at Department of Chemistry and Biochemistry, University of San Diego, California, USA
[6]Atmospheric Sciences and Global Change Division, Pacific Northwest National Laboratory, Richland, Washington, USA
[7]Now at Institute for Meteorology and Climate Research, Karlsruhe Institute of Technology, Germany
[8]Division of Atmospheric and Oceanic Sciences, University of California at Los Angeles, California, USA
[9]Laboratory of Atmospheric Chemistry, Paul Scherrer Institute, Switzerland
*Corresponding author phone: 858-534-4852; fax: 858-534-4851; email: lmrussell@ucsd.edu

S1 Similarity metric

Values of the cosine angle metric (Equation 1, Section 2.4) between ambient particle and reference spectra are shown in Figure S1. Larger values indicate greater similarity (greater proximity in feature vector space).

S2 Resolution of BC + α-pinene SOA

We present two trials for which we try to separate the spectral contribution of BC seed aerosol from the α-pinene SOA to isolate the spectral profile of the latter component. One approach is a simple scaling method (Section S2.1), and the other is a constrained nonlinear least squares fitting of a layered model (Section S2.2).

S2.1 Simple scaling

We first scale the reference BC spectra — either Highly-Oriented Pyrolitic Graphite (HOPG) or soot generated from a methane flame from Hopkins et al. (2007) — to BC + α-pinene SOA aerosol to averaged spectra from two selected particles (Figure S2). The maximum amount of scaling allowed is determined by the minimum of $s_{mixed}(\lambda)/s_{BC}(\lambda)$ for all λ, where $s_{mixed}(\lambda)$ and $s_{BC}(\lambda)$ are the spectra of the BC + α-pinene SOA and BC reference spectra, respectively, such that no part of residual spectra is negative. As shown in Figure S2, the residual absorbance for all cases lacks characteristic features of organic aerosol spectra (Takahama et al., 2007; Hopkins et al., 2007; Tivanski et al., 2007; Moffet et al., 2010), suggesting that the scaling is not very realistic.

S2.2 Layered model

We present an alternative method by which we assume a linear combination of BC and SOA spectra according to a layerd model (Takahama et al., 2010). Let

R_p = particle radius
R_c = inner core radius
r = radial distance
λ = energy
$i = \{1, 2, \ldots, m\}$ = radial index
$j = \{1, 2, \ldots, n\}$ = spectral index

$\mathbf{S}_p = \left[s_{p,ij}\right]$; $s_{p,ij} = \mathrm{s}_p(r_i, \lambda_j)$ = average particle spectra for each annulus at radius $r_i \pm \delta r_i$
$\mathbf{s}_c = \left[s_{c,j}\right]$; $s_{c,j} = \mathrm{s}_c(\lambda_j)$ = inner core spectra
$\mathbf{s}_o = \left[s_{o,j}\right]$; $s_{o,j} = \mathrm{s}_o(\lambda_j)$ = outer layer spectra
$\mathbf{t}_c = \left[t_{c,i}\right]$; $t_{c,i} = \mathrm{t}_c(r_i)$ = inner core thickness
$\mathbf{t}_o = \left[t_{o,i}\right]$; $t_{o,i} = \mathrm{t}_o(r_i)$ = outer layer thickness
$\mathbf{E} = \left[e_{ij}\right]$; $e_{ij} = \mathrm{e}(r_i, \lambda_j)$ = residual

We examine the case for two approximately spherical particles (same particles selected previously for the simple scaling method). Variations in optical thickness as a function of particle radius are defined by (Takahama et al., 2010) (reformulated here without trigonometric functions): $r = [0, R_p]$; R_p is a fixed value estimated from image geometry; R_c is degree of freedom in absence of additional/external information.

$$\begin{aligned} \mathrm{t}_p(r) &= 2\sqrt{R_p^2 - r^2} \\ \mathrm{t}_c(r) &= \begin{cases} 2\sqrt{R_c^2 - r^2} & \text{if } r \leq R_c \\ 0 & \text{otherwise} \end{cases} \\ \mathrm{t}_o(r) &= \mathrm{t}_p(r) - \mathrm{t}_c(r) \end{aligned} \tag{S1}$$

We wish to find $\mathrm{s}_c(\lambda)$ which best explains the observed spectra $\mathrm{s}_p(r, \lambda)$, when combined with $\mathrm{s}_o(\lambda)$ in proportion to layer thicknesses over a range of radial distances. Correctly assuming that our reference spectrum is scaled arbitrarily, we introduce an adjustable factor, a_c:

$$\mathrm{s}_p(r_i, \lambda_j) = a_c\, \mathrm{t}_c\Big|_{R_c}(r_i)\, \mathrm{s}_c(\lambda_j) + \mathrm{t}_o\Big|_{R_p, R_c}(r_i)\, \mathrm{s}_o(\lambda_j) + \mathrm{e}(r_i, \lambda_j) \qquad \begin{array}{c} \forall\ i = \{1, 2, \ldots, m\}\ \vee \\ j = \{1, 2, \ldots, n\} \end{array} \tag{S2}$$

Vertical bars with subscripts indicate implicit parameters. In matrix form, the equality above and the problem statement which follows can be restated as finding $\mathbf{s}_o$ (of dimension $n \times 1$) from $\mathbf{s}_c$ (also of dimension $n \times 1$) and $\mathbf{S}_p$ (of dimensions $m \times n$):

$$\mathbf{S}_p = a_c \mathbf{t}_c \mathbf{s}_c^T + \mathbf{t}_o \mathbf{s}_o^T + \mathbf{E}\ . \tag{S3}$$

The thickness at each radius, r, provides an additional constraint to the proportion in which two components are combined. We find a_c and R_c in addition to $\mathbf{s}_o$, subject to non-negativity constraints:

$$\{\mathbf{s}_o, a_c, R_c\} = \underset{\mathbf{s}_o, a_c, R_c}{\arg\min} \sum_i \sum_j e_{ij} \tag{S4}$$

where

$$\begin{aligned} &\mathbf{s}_o \geq \mathbf{0} \\ &a_c > 0 \\ &0 \leq R_c < R_p \end{aligned}$$

In contrast to the work of Lanz et al. (2008) in which known and unknown spectral profiles were combined in a factor-analytic decomposition using the Multi-Linear Engine (ME-2, Paatero et al., 2002), Equation (S4) can be solved with constrained non-linear least squares as rotational ambituity is eliminated through

the specification of optical thicknesses. Therefore, we solve this minimization problem with the Levenberg-Marquardt algorithm.

The selection of radial distances at which we sample the annular spectra are not trivial, as we wish to examine spectra from a series of annuli in which $\mathbf{s}_c$ and $\mathbf{s}_o$ are combined in varying proportions. $\nabla_r \mathrm{s}_p(r,\lambda)$ increases rapidly as $r \to R_p$; ${\nabla_r}^{t_c(r)}/_{t_o(r)}$ increases rapidly as $r \to R_c$, but the contribution from $\mathbf{s}_c$ necessarily drops to zero when $r > R_c$ (and we do not know R_c a priori). To capture the variations in which absorbance due to variation in thickness, we select a set of radii on two sets of criteria to increase the sample number under both cases, where $r \to R_p$ and $r \leq R_c$ ($\mathcal{R}_{\mathrm{inv}}$ and $\mathcal{R}_{\mathrm{lin}}$, respectively), and combine the two (as $\mathcal{R}$) in our final specification.

$$\begin{aligned} \mathcal{R}_{\mathrm{inv}} &= \left\{ R_p \sqrt{1 - \left(\frac{i}{N-1}\right)^2} : i = 0, 1, \ldots, N-1 \right\} \\ \mathcal{R}_{\mathrm{lin}} &= \left\{ R_p \left(\frac{i}{N-1}\right) : i = 0, 1, \ldots, N-1 \right\} \\ \mathcal{R} &= \mathcal{R}_{\mathrm{inv}} \cup \mathcal{R}_{\mathrm{lin}} \end{aligned} \tag{S5}$$

We set $N = 20$ for both $\mathcal{R}_{\mathrm{inv}}$ and $\mathcal{R}_{\mathrm{lin}}$, and the positions of combined radial distances, $\mathcal{R}$, are illustrated by colored lines in Figures S3a-d. The selection of radial distances can be revised through iteration, but a single iteration is sufficient for us to propose a conclusion to explain our observations.

The scaled BC reference spectra ($\mathbf{s}_c$) and outer layer spectra ($\mathbf{s}_o$) are shown in Figures S4a-d. The effectively undetectable core size (particle in column 1) and variation in estimated core sizes dependent on BC reference spectra used (particle in column 2) essentially suggest that the aromaticity in the outer layer is still high, indicating an incomplete separation between the BC and SOA. This is likely to be a physical rather than purely mathematical phenomena, as supported by Figures S3c-f (which are invariant with respect to fitting). In both particles, the absorbance at 285 eV normalized by the total carbon content (Takahama et al., 2010) does not decrease as a function of radial distance (Figures S3c,d), which is inconsistent with what we would expect if the BC is clustered at the center or core of the mixed particle. Furthermore, the outermost layer shown by the darkest red spectra (Figures S3e,f) still contains significant aromaticity. The relative invariance with respect to radial distance also holds true for the carboxylic carbonyl absorbance at 289 eV (Figures S3c,d; carboxylic acids are observed as abundant products of α-pinene oxidation; Yu et al., 1999).

S2.3 Interpretation

While the disturbance of particle morphology or chemical distribution upon impaction to the substrate cannot be ruled out, a distributed (non-core-shell) configuration of BC mixed with secondary aerosol has also been reported previously (Adachi and Buseck, 2008; Sedlacek et al., 2012; Thompson et al., 2012) for ambient particles with high-resolution TEM and SP2. From the application of two separate approaches to STXM-NEXAFS measurements (Sections S2.1 and S2.2), we also find that it is likely that the α-pinene SOA and BC are not segregated into a core-shell morphology within the mixed particles (BC + α-pinene SOA).

References

Adachi K. and Buseck P. R. (2008). Internally mixed soot, sulfates, and organic matter in aerosol particles from Mexico City. *Atmos. Chem. Phys.*, 8(21):6469–6481, doi: 10.5194/acp-8-6469-2008.

Hopkins, R. J., Lewis, K., Desyaterik, Y., Wang, Z., Tivanski, A. V., Arnott, W. P., Laskin, A., and Gilles, M. K. (2007). Correlations between optical, chemical and physical properties of biomass burn aerosols. *Geophy. Res. Lett.*, 34(18):L18806, doi: 10.1029/2007GL030502.

Lanz, V. A., Alfarra, M. R., Baltensperger, U., Buchmann, B., Hueglin, C., Szidat, S., Wehrli, M. N., Wacker, L., Weimer, S., Caseiro, A., Puxbaum, H., and Prévôt, A. S. H. (2008). Source attribution of submicron organic aerosols during wintertime inversions by advanced factor analysis of aerosol mass spectra. *Environ. Sci. & Tech.*, 42(1):214–220, doi: 10.1021/es0707207.

Moffet, R. C., Henn, T., Laskin, A., and Gilles, M. K. (2010). Automated chemical analysis of internally mixed aerosol particles using x-ray spectromicroscopy at the carbon k-edge. *Anal. Chem.*, 82(19):7906–7914, doi: 10.1021/ac1012909.

Paatero, P., Hopke, P. K., Song, X. H., and Ramadan, Z. (2002). Understanding and controlling rotations in factor analytic models. *Chem. Intell. Lab. Sys.*, 60(1-2):253–264, doi: 10.1016/S0169-7439(01)00200-3.

Sedlacek, A. J., Lewis, E. R., Kleinman, L., Xu, J., and Zhang, Q. (2012). Determination of and evidence for non-core-shell structure of particles containing black carbon using the single-particle soot photometer (sp2). *Geophys. Res. Lett.*, 39:L06802, doi: 10.1029/2012GL050905.

Takahama, S., Gilardoni, S., Russell, L. M., and Kilcoyne, A. L. D. (2007). Classification of multiple types of organic carbon composition in atmospheric particles by scanning transmission x-ray microscopy analysis. *Atmospheric Environment*, 41(40):9435–9451, doi: 10.1016/j.atmosenv.2007.08.051.

Takahama, S., Liu, S., and Russell, L. M. (2010). Coatings and clusters of carboxylic acids in carbon-containing atmospheric particles from spectromicroscopy and their implications for cloud-nucleating and optical properties. *J. Geophys. Res.*, 115:D01202, doi: 10.1029/2009JD012622.

Thompson, J. E., Hayes, P. L., Jimenez, J. L., Adachi, K., Zhang, X., Liu, J., Weber, R. J., and Buseck, P. R. (2012). Aerosol optical properties at pasadena, ca during calnex 2010. *Atmos. Environ.*, 55(0):190 – 200, doi: 10.1016/j.atmosenv.2012.03.011.

Tivanski, A. V., Hopkins, R. J., Tyliszczak, T., and Gilles, M. K. (2007). Oxygenated interface on biomass burn tar balls determined by single particle scanning transmission x-ray microscopy. *J. Phys. Chem. A*, 111(25):5448–5458. doi: 10.1021/jp070155u.

Yu, J. Z., Cocker, D. R., Griffin, R. J., Flagan, R. C., and Seinfeld, J. H. (1999). Gas-phase ozone oxidation of monoterpenes: Gaseous and particulate products. *J. Atmos. Chem.*, 34(2):207–258, doi: 10.1023/A:1006254930583.

Figures

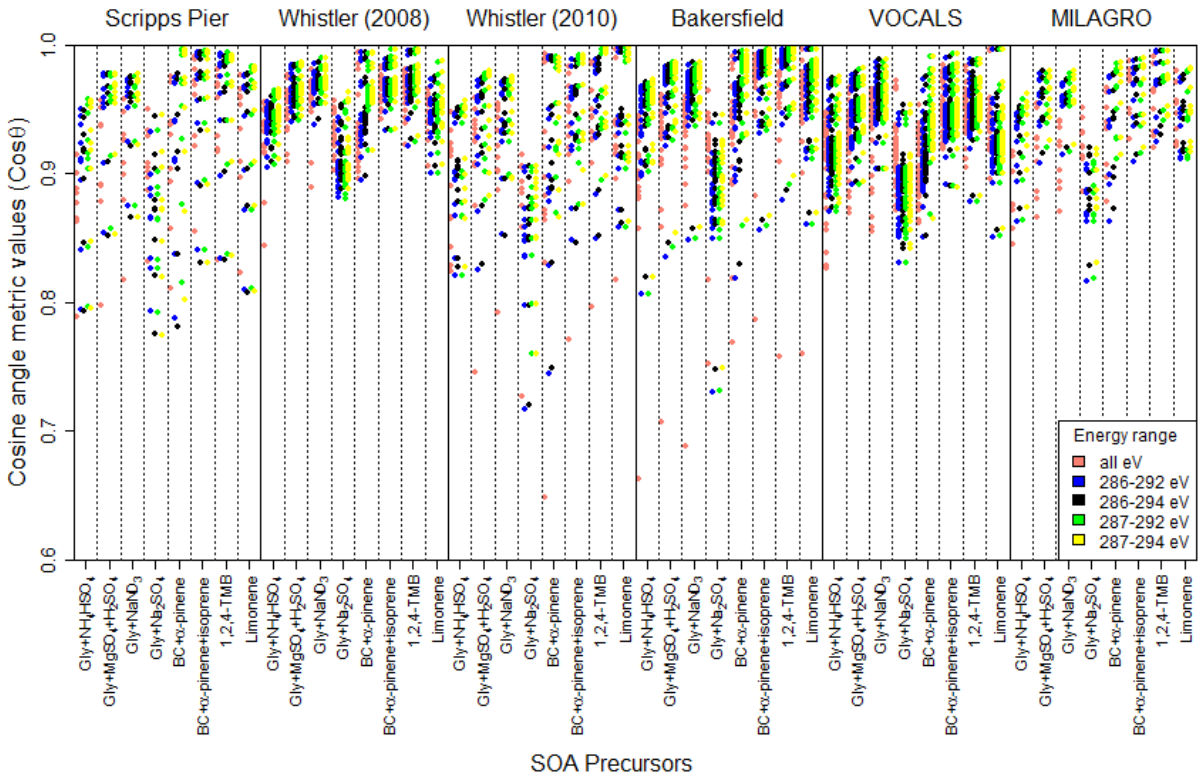

Figure S1: Cosine angle metric values calculated for different energy ranges among spectra of ambient particles and SOA particles from various precursors.

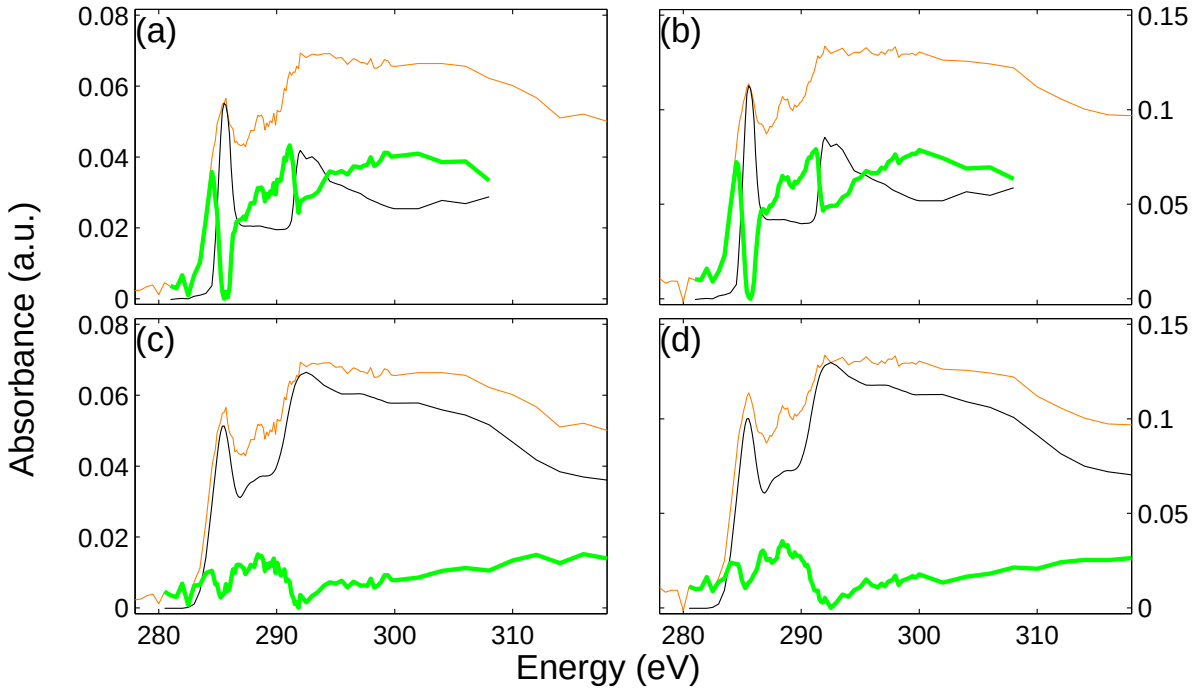

Figure S2: Particle spectra (orange line), scaled reference spectra (black line; a and b: HOPG; c and d: methane soot), and residual spectra (green line) from simple scaling for two particles (shown in separate columns).

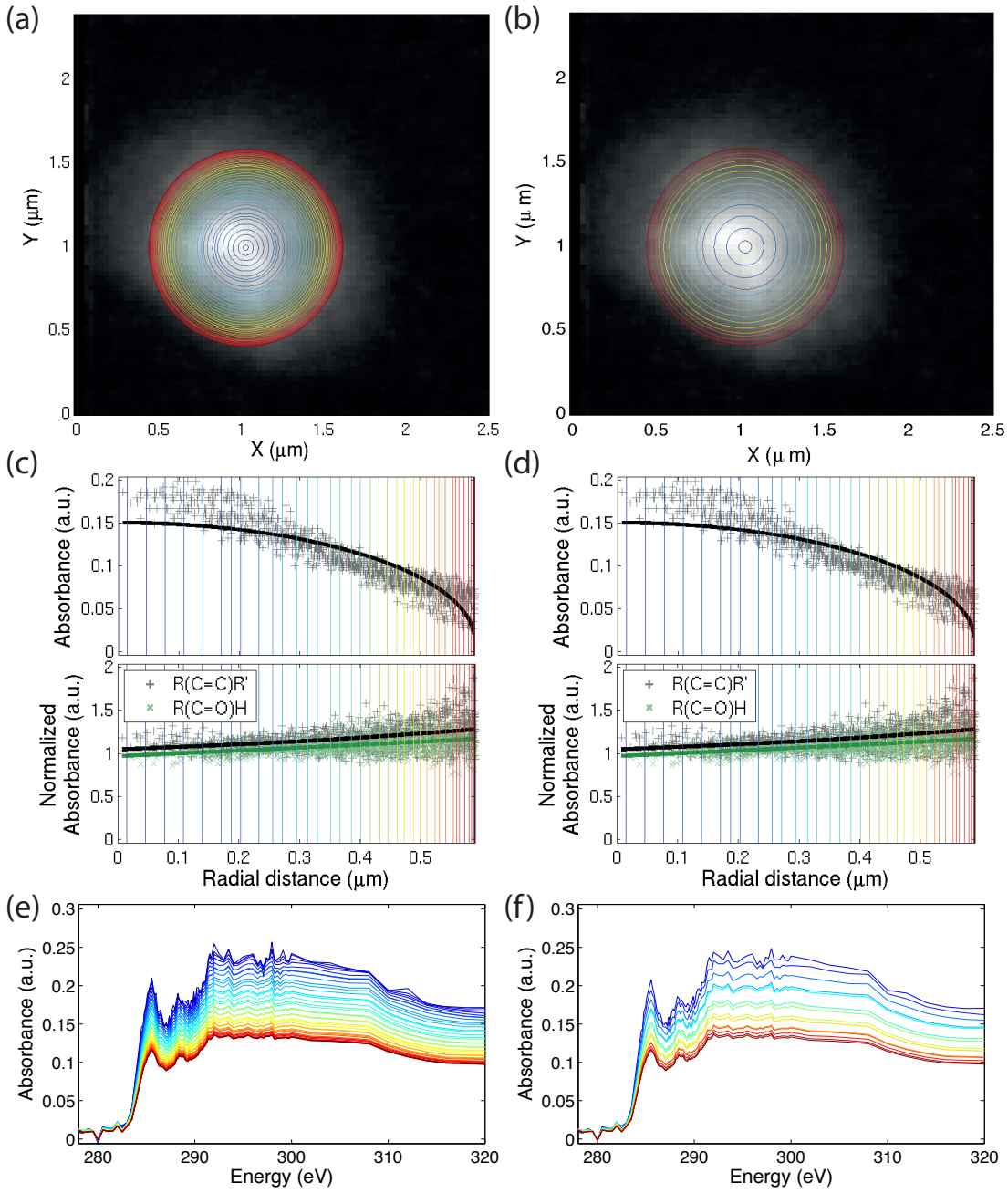

Figure S3: Characterization of particle absorbance and spectra as a function of radial distance. Each column contains information regarding one particle. Top row: particle images (white indicates higher absorbance); second row: absolute absorbance at 289 eV and absorbances at 285 eV [aromatic, R(C=C)R'; gray points and black line] and 289 eV [carboxylic carbonyl, R(C=O)H; green points and green line] normalized by total carbon absorbance (mean of 305 to 320 eV; Takahama et al., 2010) as a function of radial distance; bottom row: absorbance spectra at various radial distances. Line colors correspond to same set of discretized radial distances (Equation S5) in all three sets of images.

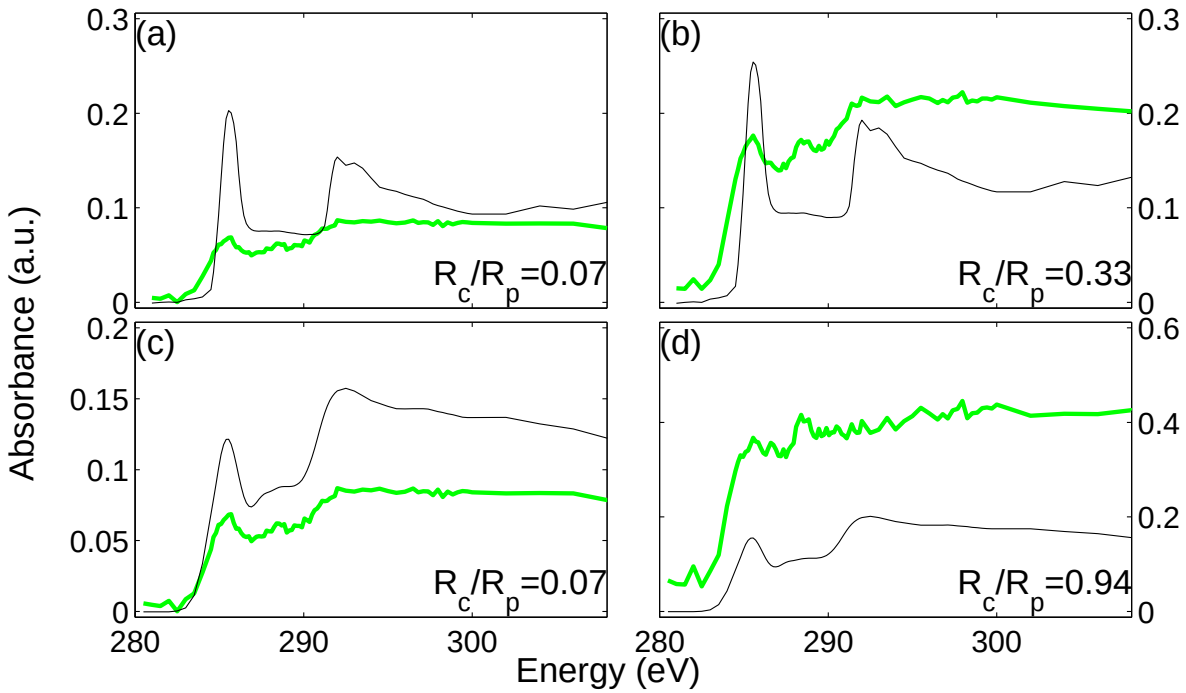

Figure S4: Results of spectral fitting from Equations (S3) and (S4). Each column contains information regarding one particle. Top row: results from fitting with HOPG reference spectra; bottom row: results from fitting with methane soot reference spectra. Shown are the BC reference spectra assumed for $\mathbf{s}_c$ (black lines), outer layer spectra $\mathbf{s}_o$ (green lines), and the core:particle radius ratio.